Table 3 Factors associated with the response to peginterferon-α (PEG-IFN) and ribavirin

	SVR 29 cases	NR 38 cases	*P*-value
Age	52.8 ± 11.0	59.8 ± 6.4	0.002
Gender (male)	17 (58%)	20 (52%)	0.625
BMI (kg/m^2)	23.9 ± 3.1	22.9 ± 3.1	0.190
Viral load (KIU/mL)	2188 ± 1764	2420 ± 1689	0.587
White blood cell (/uL)	4816 ± 1427	5225 ± 1287	0.242
Hemoglobin (mg/dL)	14.1 ± 1.1	14.0 ± 1.3	0.626
Platelet (×10^3/uL)	176.5 ± 52.8	160.3 ± 89.2	0.350
AST (IU/L)	75.5 ± 36.1	78.3 ± 51.5	0.795
ALT (IU/L)	108.9 ± 56.8	95.3 ± 56.0	0.333
γGTP (IU/L)	63.9 ± 61.9	75.7 ± 68.6	0.464
Core 70 wild	20 (69%)	20 (53%)	0.176
Core 91 wild	21 (72%)	29 (71%)	0.173
IL28 TT rs8099917	26 (90%)	25 (65%)	0.022
steatosis	14 (47%)	23 (61%)	0.452
Activity (severe)†	10 (34%)	21 (64%)	0.091
Fibrosis (severe)‡	18 (62%)	27 (71%)	0.437
SOCS3 (Positive)	8 (27%)	23 (61%)	0.015

†Severe activity was defined as A2 or A3.
‡Severe fibrosis was defined as F2, F3, or F4.
ALT, alanine aminotransferase; AST, aspartate aminotransferase; BMI, body mass index; γGTP, gamma-glutamyl transpeptidase; HCV, hepatitis C virus; NR, non responder; SOCS3, suppressor of cytokine signal 3; SVR, sustained virological response.

type 1.[13–15] We previously reported that SOCS3 was a factor associated with the response to PEG-IFN treatment.[16] We compared these factors and clarified their usefulness as predictors of PEG-IFN plus combination therapy.

In the laboratory data from our patients, a significant difference between the groups with weak and strong SOCS3 staining was found in the level of AST, ALT, and platelets. These laboratory data suggested that the SOCS3 immunostained area was significantly associated with the presence of inflammation and the fibrosis stage. Indeed, in a pathological study, the inflammation and fibrosis stage were significantly different between the low and high SOCS3 immunostaining groups. This finding was consistent with our previous study that showed that the SOCS3 immunostained area was influenced by inflammation and the fibrosis stage.[16]

Table 4 Results of a multilogistic regression analysis

	Odds ratio	*P*-value
Age (>65 years)	0.221 (0.120–0.966)	0.045
IL28 TT	5.422 (1.254–23.617)	0.024
SOCS3 (low)	0.308 (0.104–0.948)	0.040

SOCS3, suppressor of cytokine signal 3.

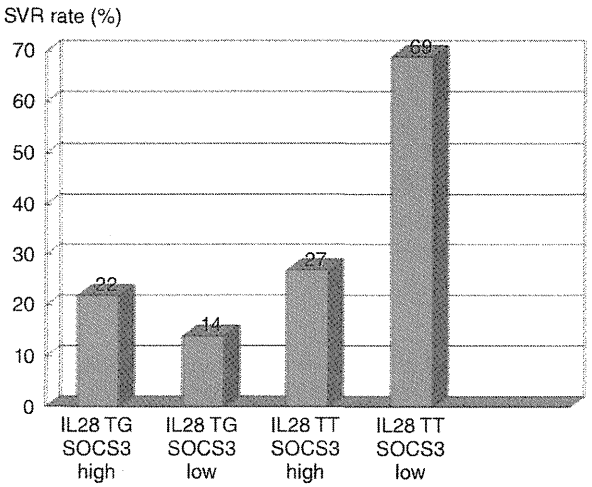

Figure 3 A total of 12.5% of patients with IL28 TG and suppressor of cytokine signaling 3 (SOCS3) high immunostaining showed a sustained virological response (SVR), 20% of patients with IL28 TG and SOCS3 low immunostaining, 31% of patients with IL28 TT and SOCS3 high immunostaining, and 68% of patients with IL28 TG and SOCS3 low immunostaining showed a SVR.

Moreover, a significant difference between the low and high SOCS3 groups was also found in the level of γGTP. Several previous reports showed that the level of γGTP was correlated with steatosis in the liver.[7,17] In this study, the presence of steatosis also was significantly different in the low and high SOCS3 immunostaining groups. Together with our results, these results demonstrated that the SOCS3 immunostained area in the liver was associated with obesity, insulin resistance, and hepatic steatosis.[18,19]

Although recent reports showed that genetic variation of IL28B was also associated with liver inflammation and fibrosis,[20] this was not associated with the SOCS3 immunostained area in the present study. The SOCS3 proteins are known for their role as negative regulators and inhibitors of Janus kinase-signal transducer and activator of transcription (JAK-STAT) signaling, where they mediate a classical negative feedback loop in the IFN-α/β receptor signaling pathway.[21,22] The mechanism that leads to the association between genetic variation of IL28B and the effect of interferon therapy is clear, because it has been demonstrated that IL28B inhibits hepatitis C virus replication through the JAK-STAT pathway.[23] Taken together, both the SOCS3 immunostained area and IL28B polymorphisms were associated with the JAK-STAT pathway, but the different factors might interfere with JAK-STAT signaling in different ways.

The NR rate to combination PEG-IFN plus ribavirin therapy in patients with the non-TT genotype was 10–20%. The value of NR for the prediction of the genetic variation of IL28B was therefore very high. On the other hand, the SVR rate in patients with the TG genotype was about 50%. The value of SVR prediction based only on the genetic variation of IL28B was therefore not as strong for this genotype.

The substitution of core amino acids was also reported to be a predictive factor for the response to interferon therapy and was significantly associated with the genetic variation of IL28B.[24] On the other hand, the SOCS3 immunostained area was independent of both of these factors. Thus, we suggested that using a combination of the SOCS3 immunostained area with the IL28B genotype can provide the best prediction of the response to PEG-IFN plus ribavirin therapy.

Indeed, in TT genotype patients, the SVR rate in the SOCS3 weak group was about 70%, and NVR rate in the SOCS3 low immunostained group was 27%. If a liver biopsy was performed, immunostaining for SOCS3 was easy, and provided a useful predictor of the response to interferon therapy.

Our study has some limitations. Our sample size was too small. Further large-scale studies are necessary to confirm the present results and to provide a better understanding of the interactions between the SOCS3 immunostained area and the genetic variation of IL28B.

In conclusion, a combination of the SOCS3 immunostained area in the liver and the assessment of the genetic variation of IL28B seem to be good predictors of the response to PEG-IFN plus ribavirin therapy.

REFERENCES

1 Mangia A, Ricci GL, Persico M *et al.* A randomized controlled trial of pegylated interferon alpha-2a (40 KD) or interferon alpha-2a plus ribavirin and amantadine vs interferon alpha-2a and ribavirin in treatment-naive patients with chronic hepatitis C. *J Viral Hepat* 2005; **12**: 292–9.
2 Akuta N, Suzuki F, Kawamura Y *et al.* Predictive factors of early and sustained responses to peginterferon plus ribavirin combination therapy in Japanese patients infected with hepatitis C virus genotype 1b: amino acid substitutions in the core region and low-density lipoprotein cholesterol levels. *J Hepatol* 2007; **46**: 403–10.
3 Wedemeyer H, Wiegand J, Cornberg M, Manns MP. Polyethylene glycol-interferon: current status in hepatitis C virus therapy. *J Gastroenterol Hepatol* 2002; **17** (Suppl 3): S344–50.
4 Davis GL, Esteban-Mur R, Rustgi V *et al.* Interferon alfa-2b alone or in combination with ribavirin for the treatment of relapse of chronic hepatitis C. International Hepatitis Interventional Therapy Group. *N Engl J Med* 1998; **339**: 1493–9.
5 Poynard T, Marcellin P, Lee SS *et al.* Randomised trial of interferon alpha2b plus ribavirin for 48 weeks or for 24 weeks versus interferon alpha2b plus placebo for 48 weeks for treatment of chronic infection with hepatitis C virus. International Hepatitis Interventional Therapy Group (IHIT). *Lancet* 1998; **352**: 1426–32.
6 Bressler BL, Guindi M, Tomlinson G, Heathcote J. High body mass index is an independent risk factor for nonresponse to antiviral treatment in chronic hepatitis C. *Hepatology* 2003; **38**: 639–44.
7 Yaginuma R, Ikejima K, Okumura K *et al.* Hepatic steatosis is a predictor of poor response to interferon alpha-2b and ribavirin combination therapy in Japanese patients with chronic hepatitis C. *Hepatol Res* 2006; **35**: 19–25.
8 Zografos TA, Liaskos C, Rigopoulou EI *et al.* Adiponectin: a new independent predictor of liver steatosis and response to IFN-alpha treatment in chronic hepatitis C. *Am J Gastroenterol* 2008; **103**: 605–14.
9 Yamada G, Iino S, Okuno T *et al.* Virological response in patients with hepatitis C virus genotype 1b and a high viral load: impact of peginterferon-alpha-2a plus ribavirin dose reductions and host-related factors. *Clin Drug Investig* 2008; **28**: 9–16.

10 Iwasaki Y, Ikeda H, Araki Y *et al.* Limitation of combination therapy of interferon and ribavirin for older patients with chronic hepatitis C. *Hepatology* 2006; **43**: 54–63.
11 Enomoto N, Sakuma I, Asahina Y *et al.* Mutations in the nonstructural protein 5A gene and response to interferon in patients with chronic hepatitis C virus 1b infection. *N Engl J Med* 1996; **334**: 77–81.
12 Akuta N, Suzuki F, Hirakawa M *et al.* Association of amino acid substitution pattern in core protein of hepatitis C virus genotype 2a high viral load and virological response to interferon-ribavirin combination therapy. *Intervirology* 2009; **52**: 301–9.
13 Tanaka Y, Nishida N, Sugiyama M *et al.* Genome-wide association of IL28B with response to pegylated interferon-alpha and ribavirin therapy for chronic hepatitis C. *Nat Genet* 2009; **41**: 1105–9.
14 Thomas DL, Thio CL, Martin MP *et al.* Genetic variation in IL28B and spontaneous clearance of hepatitis C virus. *Nature* 2009; **461**: 798–801.
15 Suppiah V, Moldovan M, Ahlenstiel G *et al.* IL28B is associated with response to chronic hepatitis C interferon-alpha and ribavirin therapy. *Nat Genet* 2009; **41**: 1100–4.
16 Miyaaki H, Ichikawa T, Nakao K *et al.* Predictive value of suppressor of cytokine signal 3 (SOCS3) in the outcome of interferon therapy in chronic hepatitis C. *Hepatol Res* 2009; **39**: 850–5.
17 Ikai E, Ishizaki M, Suzuki Y, Ishida M, Noborizaka Y, Yamada Y. Association between hepatic steatosis, insulin resistance and hyperinsulinaemia as related to hypertension in alcohol consumers and obese people. *J Hum Hypertens* 1995; **9**: 101–5.
18 Walsh MJ, Jonsson JR, Richardson MM *et al.* Non-response to antiviral therapy is associated with obesity and increased hepatic expression of suppressor of cytokine signalling 3 (SOCS-3) in patients with chronic hepatitis C, viral genotype 1. *Gut* 2006; **55**: 529–35.
19 Ueki K, Kondo T, Tseng YH, Kahn CR. Central role of suppressors of cytokine signaling proteins in hepatic steatosis, insulin resistance, and the metabolic syndrome in the mouse. *Proc Natl Acad Sci U.S.A.* 2004; **101**: 10422–7.
20 Abe H, Ochi H, Maekawa T *et al.* Common variation of IL28 affects gamma-GTP levels and inflammation of the liver in chronically infected hepatitis C virus patients. *J Hepatol* 2010; **53**: 439–43.
21 Alexander WS. Suppressors of cytokine signalling (SOCS) in the immune system. *Nat Rev Immunol* 2002; **2**: 410–6.
22 Yasukawa H, Sasaki A, Yoshimura A. Negative regulation of cytokine signaling pathways. *Annu Rev Immunol* 2000; **18**: 143–64.
23 Zhang L, Jilg N, Shao RX *et al.* IL28B inhibits Hepatitis C virus replication through the JAK-STAT pathway. *J Hepatol* 2011; **55**: 289–98.
24 Akuta N, Suzuki F, Hirakawa M *et al.* Amino acid substitution in hepatitis C virus core region and genetic variation near the interleukin 28B gene predict viral response to telaprevir with peginterferon and ribavirin. *Hepatology* 2010; **52**: 421–9.

Cancer Letters 310 (2011) 25–34

Contents lists available at ScienceDirect

Cancer Letters

journal homepage: www.elsevier.com/locate/canlet

N-myc downstream regulated gene1/Cap43 overexpression suppresses tumor growth by hepatic cancer cells through cell cycle arrest at the G_0/G_1 phase

Jun Akiba [a,*,1], Yuichi Murakami [b,1], Masaki Noda [b], Kosuke Watari [b], Sachiko Ogasawara [a], Takafumi Yoshida [c], Akihiko Kawahara [d], Sakiko Sanada [a], Makiko Yasumoto [a], Rin Yamaguchi [a], Masayoshi Kage [d], Michihiko Kuwano [e], Mayumi Ono [b], Hirohisa Yano [a]

[a] Department of Pathology, Kurume University School of Medicine, 67 Asahi-machi, Kurume 830-0011, Japan
[b] Department of Pharmaceutical Oncology, Graduate School of Pharmaceutical Sciences, Kyushu University, 3-1-1 Maidashi, Higashi-ku, Fukuoka 812-8582, Japan
[c] Department of Medicine, Division of Gastroenterology, Kurume University School of Medicine, 67 Asahi-machi, Kurume 830-0011, Japan
[d] Department of Diagnostic Pathology, Kurume University Hospital, 67 Asahi-machi, Kurume 830-0011, Japan
[e] Laboratory of Molecular Cancer Biology, Graduate School of Pharmaceutical Sciences, Kyushu University, 3-1-1 Maidashi, Higashi-ku, Fukuoka 812-8582, Japan

ARTICLE INFO

Article history:
Received 10 December 2010
Received in revised form 24 May 2011
Accepted 30 May 2011

Keywords:
NDRG1/Cap43
Hepatocellular carcinoma
Cell cycle arrest
p21
Cyclin dependent kinase 4

ABSTRACT

N-myc downstream regulated gene-1 (NDRG1)/Cap43 regulates tumor growth and metastasis in various carcinomas. In this study we examined whether and how NDRG1/Cap43 modulates tumor growth by human hepatocellular carcinoma (HCC) cells. NDRG1/Cap43 cDNA was used to transfect HCC cell lines (KIM-1), and stable transfectants overexpressing NDRG1/Cap43 (KIM-1/Cap43) were obtained. Cell cycle analysis showed that KIM-1/Cap43 cells were arrested in the G_0/G_1 phase. Western blot analysis demonstrated an increase in p21 in KIM-1/Cap43 cells in culture under full confluency as compared with KIM-1/Mock. When KIM-1 cells, which are very low in NDRG1/Cap43 expression, were treated with mimosine, a G_0/G_1 cell cycle blocker, expression of NDRG1/Cap43 was induced in a dose dependent manner, together with p21 induction and CDK4 reduction. *In vivo*, KIM-1/Cap43 cells showed markedly decreased tumor growth rates compared with those of KIM-1/Mock. Immunohistochemical staining demonstrated markedly higher p21 labeling index in the KIM-1/Cap43 tumor than KIM-1/Mock tumor, and lower CDK4 and Ki-67 labeling index in the KIM-1/Cap43 than KIM-1/Mock. In order to confirm suppressive effects of NDRG1/Cap43, we further established a stable transfectant expressing NDRG1/Cap43 (HAK-1B/Cap43) using another HCC cell line, HAK-1B. Western blot analysis demonstrated an increase in p21 and a decrease in CDK4 in HAK-1B/Cap43 cells in culture under full confluency as compared with HAK-1B/Mock. HAK-1B/Cap43 also showed decreased tumor growth rates as compared with its control counterpart *in vivo*. NDRG1/Cap43 overexpression thus induced cell cycle arrest at the G_0/G_1 phase accompanied by increased p21 and decreased CDK4 expression in HCC cells. NDRG1/Cap43 might play a key role in the cell cycle control of G_0/G_1 in HCC cells.

1. Introduction

Hepatocellular carcinoma (HCC) is the third most common cause of cancer death in the world. HCC is frequently associated with hepatitis B virus (HBV) – or hepatitis C virus (HCV)-induced chronic hepatitis, α-1-antitrypsin

* Corresponding author. Tel.: +81 942 31 7546; fax: +81 942 32 0905.
E-mail address: akiba@med.kurume-u.ac.jp (J. Akiba).
[1] These authors equally contributed to this work.

0304-3835/$ - see front matter © 2011 Elsevier Ireland Ltd. All rights reserved.
doi:10.1016/j.canlet.2011.05.034

deficiency, or the prolonged ingestion of alcohol or aflatoxin. The incidence of HCC differs in different geographical regions, being high in Asia and Africa. This is correlated with the frequency distribution of HBV or HCV infection. Although HCV infection rates in the United States have been historically lower than those in Asia and Africa, it is predicted that the spread of HCV infection will lead to an increase in the incidence of HCC [1]. Advances and improvements in the screening and treatment of patients at high risk for HCC have improved the prognosis of early-stage HCC [2]. However, the prognosis of advanced HCC remains extremely poor.

N-myc downstream-regulated gene-1 (NGRG-1)/calcium-associated protein 43 kDa (Cap43) is also known as Drg-1, RTP, and RIT42. NDRG1/Cap43 expression is regulated by nickel, cobalt, oxidative stress, hypoxia, phorbol esters, vitamin A, vitamin D, steroids, histone deacetylase-targeting drugs, lysophosphatidylcholine, oncogenes and tumor suppressor gene products [3–7]. NDRG1/Cap43 has the functions of keratinocyte differentiation [8], cell cycle regulation (4), myelin sheath maintenance [9], and the attenuation of hypoxic injury in human trophoblasts [10].

NDRG1/Cap43 is widely expressed in non-neoplastic tissue within the body [11]. The levels of NDRG1/Cap43 expression are lower in breast, colorectal, and prostate cancer cells than in non-neoplastic tissue, and those in prostate and pancreatic cancer are negatively correlated with the histological grade of malignancy [4,12–14]. NDRG1/Cap43 shows an inhibitory effect on the metastasis of prostate, colorectal, and breast cancer [12,15,16]. On the other hand, NDRG1/Cap43 serves as an indicator of a poor prognosis in cervical adenocarcinoma and HCC [17–19]. In our immunohistochemical study, NDRG1/Cap43 expression was increased in advanced HCC, and was overexpressed in patients with portal vein invasion or intrahepatic metastasis [19]. A study by Yan et al. has reported that the NDRG1/Cap43 knockdown by its cognate siRNA inhibited tumor cell proliferation and invasion by HCC cells [20]. In our present study, we examined whether NDRG1/Cap43 overexpression could affect tumor growth by HCC cells. The suppressive effect of NDRG1/Cap43 on the tumor growth by HCC cells is discussed in its close association with cell cycle arrest.

2. Materials and methods

2.1. Cell lines, cell culture and antibodies

Six human HCC cell lines originally established in our laboratory were used in this study: KIM-1, KYN-1, KYN-2, KYN-3, HAK-1A and HAK-1B. These cell lines were previously confirmed to retain the morphological and functional characteristics of original HCC. The cells were grown in culture medium consisting of Dulbecco's modified Eagle medium (Nissui Seiyaku Co., Japan) supplemented with 5% heat-inactivated (56 °C, 30 min) fetal bovine serum (Biosserum, Victoria, Australia), 100 U/mL penicillin, 100 mg/mL streptomycin (Gibco BRL/Life Technologies, Inc., Gaithersburg, MD, USA), and 12 mM sodium bicarbonate in a humidified atmosphere of 5% CO_2 at 37 °C. The anti-NDRG1/Cap43 antibody was generated as described previously [14]. Other antibodies were purchased as follows: anti-cyclin A, cyclin B1, cyclin E, p16, p21, cyclin dependent kinase (CDK) 1/CDC2, CDK2, CDK4, epithelial growth factor receptor (EGFR), phospho-HER3(pHER3), IκBα, phospho-IκBα (pIκBα)(Cell Signaling Technology, Danvers, MA, USA); anti-CDC6 (Proteintech Group Inc., Chicago, IL, USA); anti-phospho-EGFR (pEGFR) (Calbiochem, Darmstadt, Germany); anti-HER2, phospho-HER2 (pHER2)(Upstate Biotechnology, Bedford, MA, USA); anti-βactin (Abcam, Cambridge, MA, USA); anti-Ki-67 (Novocastra, Newcastle, UK).

2.2. Expression vector construction and transfection

NDRG1/Cap43 cDNA was amplified by reverse transcription-PCR (RT-PCR) using the 5′ and 3′ primers 5′-CATGTCTCGGGAGATGCAGGATG-3′ and 5′-AGGCCGCCTAGCAGGAGACC-3′, respectively. Amplified NDRG1/Cap43 cDNA was ligated into the pCR2.1-TOPO vector (Invitrogen, Carlsbad, CA, USA) and transferred to the pIRESneo2 expression plasmid (pIRESneo2-Cap43). Cells were transfected with pIRESneo2-Cap43 or pIRESneo2 using LipofectAMINE 2000 (Invitrogen) following the manufacturer's protocol. Stably transfected clones were established using G418 (Invitrogen) selection.

2.3. Effects of NDRG1/Cap43 on cell proliferation

The effect of NDRG1/Cap43 on the growth of cultured cells was examined with colorimetry using a 3-(4, 5-dimethylthiazol-2-yl)-2, 5-diphenyltetrazolium bromide (MTT) assay kit (Chemicon International Inc., Temecula, CA, USA). Briefly, KIM-1 cells showing NDRG1/Cap43 overexpression (KIM-1/Cap43) and the control (KIM-1/Mock) were seeded on 96-well plates (Nunc Inc., Roskild, Denmark). After culturing for Day 2, 3 and 4, the number of viable cells was measured with ImmunoMini NJ-2300 (Nalge Nunc International, Tokyo, Japan) by setting the test wavelength at 570 nm and the reference wavelength at 630 nm. To keep the optimal density within the linear range, all experiments were performed while the cells were in the logarithmic growth phase.

2.4. Cell cycle analysis

KIM-1/Cap43 and KIM-1/Mock were cultured in serum-free culture medium for 24 h. After culturing in medium containing 10% FBS for 12 h, cells were labeled with 10 μmol/L BrdU for 30 min, fixed in 70% cold ethanol at 4 °C overnight, stained with anti-BrdU and propidium iodide (Sigma Chemical Co., St Louis, MO, USA), and then analyzed using FACScan (BD Bioscience, Bedford, MA, USA). Fixed cells were washed with PBS, subjected to double-stranded DNA denaturation treatment with 2 mol/L HCl at room temperature for 30 min, neutralized with 0.1 mol/L $Na_2B_4O_7$, washed twice with PBS, 0.5% Tween 20, and 0.5% BSA (PBS-T), incubated for 30 min at room temperature with 20 μL anti-BrdU antibody, washed with PBS-T, incubated for 30 min at room temperature with

4 μL fluorescein isothiocyanate (FITC)-conjugated goat anti-mouse immunoglobulin, and washed with PBS-T. DNA was counterstained with 5 μg/mL of propidium iodide for at least 20 min before flow cytometric analysis.

2.5. Western blot analysis

Cells were rinsed with ice-cold PBS and lysed in buffer containing 50 mmol/L Tris–HCl, 350 mmol/L NaCl, 0.1% Nonidet P-40, 5 mmol/L ethylenediaminetetraacetic acid, 50 mmol/L NaF, 0.1% sodium deoxycholate, 0.1% sodium dodecyl sulfate, 1 mmol/L phenylmethylsulfonyl fluoride, 10 μg/mL aprotinin, 10 μg/mL leupeptin and 1 mmol/L Na_3VO_4. Cell lysates were subjected to sodium dodecyl sulfate–polyacrylamide slab gel and blotted onto Immobilon membranes (Millipore Corporation, Bedford, MA, USA) as described previously [7]. After transfer, the membrane was incubated with blocking solution followed by primary antibody.

2.6. Morphological findings of culture cell

KIM-1/Cap43 or KIM-1/Mock cells were seeded on Lab-Tek Tissue Culture Chamber Slides (Nunc, Inc.), fixed in 4% paraformaldehyde for 20 min, and stained with H&E for light microscopic observation.

2.7. Mimosine, treatment in culture cell

KIM-1 cell, which is very low in NDRG-1/Cap43 expression, was treated with 10 μM to 400 μM mimosine (Sigma) for 24 h. Samples were subjected to Western blot analysis. KIM-1 was also treated without or with 200 μM and 400 μM mimosine for 24 h for cell cycle analysis.

2.8. Nude mouse xenograft experiment

Cells were suspended in sterile PBS at a concentration of 5×10^8 cells/mL, and 100 μL was injected subcutaneously into the right flank of the 4–10-week-old female BALB/c nu/nu athymic nude mice. The tumor size was measured in two directions using calipers, and the tumor volume (mm^3) was estimated using the equation: length × $(\text{width})^2 \times 0.5$. Measurement was performed every week, and changes in the average tumor volume were recorded. The mice were sacrificed after 7 weeks and the tumors were removed. Specimens were fixed in 10% formalin and embedded in paraffin blocks. Unstained 4-μm sections were cut from the blocks and stained with H&E for light microscopic observation. Immunohistochemistry for formalin-fixed paraffin-embedded sections was performed. Unstained sections were immunostained with antibodies against human NDRG1/Cap43, p21, CDK4 and Ki-67, following the method described previously [21]. All counts were performed by two independent observers (J.A. and M.Y.).

2.9. Effect of NDRG1/Cap43 in another HCC cell line overexpressing NDRG1/Cap43

To further confirm the effect of NDRG1/Cap43 overexpression on tumor growth by HCC cells *in vivo*, we established a stable NDRG1/Cap43 overexpressing cell line using different HCC cell line. HAK-1A and HAK-1B were previously established from a single HCC nodule of the well differentiated part and the dedifferentiated (poorly differentiated) part, respectively [22]. HAK-1B cells showing NDRG1/Cap43 overexpression (HAK-1B/Cap43) and the control (HAK-1B/Mock) were used following examinations. HAK-1B/Mock or HAK-1B/Cap43 cells (1×10^7) were used to inoculate 6–7-week-old male BALB/c nu/nu athymic nude mice subcutaneously, and the tumor diameters were measured every 3 days from Day 7. The tumor volume was estimated as previously described.

2.10. Statistical analysis

Data are expressed as the mean ± SD. Comparisons between groups were performed using Student's *t*-test. Differences were considered significant at $P < 0.05$.

3. Results

3.1. NDRG1/Cap43 overexpression inhibits the cell proliferation of HCC cell line KIM-1 in culture

We first compared the protein levels of NDRG1/Cap43 in four HCC cell lines. Out of the four cell lines, KYN-2 and KYN-3 showed comparable levels of NDRG1/Cap43 expression whereas there was no apparent expression of NDRG1/Cap43 in KIM-1 and KYN-1 (Fig. 1A). We next established cell line KIM-1/Cap43 by the transfection of NDRG1/Cap43 cDNA into KIM-1. KIM-1/Cap43 showed enhanced expression of NDRG1/Cap43 as compared to its parental mock transfectants, KIM-1/Mock and (Fig. 1B). We also compared the growth rates between mock and NDRG1/Cap43 transfectants of KIM-1 in the presence of 10% serum. KIM-1/Cap43 showed a significantly slower growth rate as compared with that of its parental counterpart (Fig. 1C). There were no apparent morphological differences between KIM-1/Cap43 and KIM-1/Mock (Fig. 1D).

3.2. NDRG1/Cap43 induced cell cycle arrest in the G_0/G_1 phase

We examined the cell cycle status by flowcytometric analysis.

There was relatively more cell population (60.7%) of KIM-1/Cap43 cells, in the G_0/G_1 phase than cell population (46.0%) of KIM-1/Mock cells (Fig. 2A). Since we have previously reported that NDRG1/Cap43 overexpression induced suppression of NF-κB pathway in human pancreas cancer cells [14,23], we examined the expression of IκBα and pIκBα in addition to EGFR family proteins. Expression protein levels of total and phosphorylated EGFR family proteins, IκBα and pIκBα were compared by Western blot analysis (Fig. 2B). There was no apparent difference in the expression level of EGFR, HER2 and HER3, and their phosphorylated proteins. By contrast the expression of IκBα and pIκBα was reduced in KIM-1/Cap43 as compared to KIM-1/Mock. Furthermore, Western blot analysis of cell cycle-related proteins revealed increased expression p21 in KIM-1/Cap43 under confluent culture condition. However, there was no difference in the protein levels of cyclin A, cyclin B1, cyclin E, p16, CDK1/CDC2, CDK2, CDK4 and CDC6 between KIM-1/Cap43 and KIM-1/Mock (Fig. 2C).

We next examined whether NDRG1/Cap43 overexpression was specifically associated with cell cycle at G_0/G_1 arrest. We examined the effect of a specific blocking reagent of cell cycle G_0/G_1, mimosine, on exponentially growing KIM-1 cells. Expression of NDRG1/Cap43 was markedly upregulated when exposed to various doses of mimosine at 200 μM and 400 μM for 24 h (Fig. 3A). Mimosine also induced expression p21 at

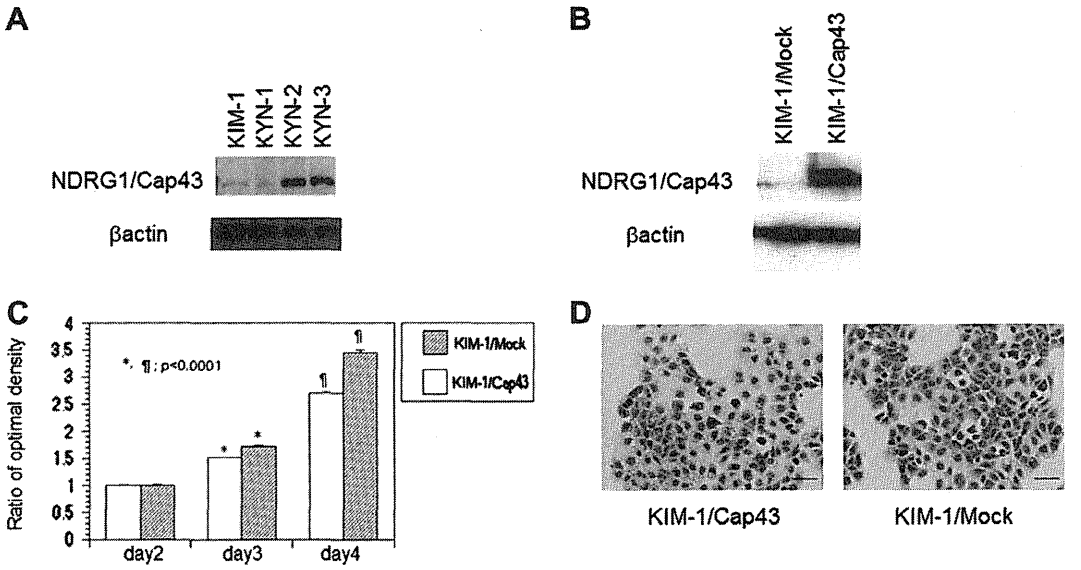

Fig. 1. Effect of NDRG1/Cap43 expression, cell proliferation, and morphological findings. (A) Expression of NDRG1/Cap43 in six HCC cell lines determined by Western blot analysis. Four cell lines out of six had NDRG1/Cap43 expression. (B) Expression of NDRG1/Cap43 in NDRG1/Cap43 and mock transfectants in KIM-1 cell line determined by Western blot analysis. (C) Comparison of cell growth between NDRG1/Cap43 and mock transfectants in KIM-1 cell line. Cell growth was measured at Day 2, 3, and 4 after seeding. Cell growth of NDRG1/Cap43 transfectant was significantly suppressed at 3 and 4 days compared with that of mock transfectant. The *Y*-axis shows the ratio of optimal density when that of Day 2 was 1.0. (D) There was no apparent morphological difference between NDRG1/Cap43 and mock transfectants. Scale bar indicates 50 μm.

200 μM and 400 μM and inhibited CDK4 expression at 400 μM (Fig. 3A). Cell cycle was specifically arrested at G_0/G_1 when KIM-1 cells were treated with 200 μM or 400 μM mimosine for 24 h (Fig. 3B).

3.3. A marked decrease in tumor growth by NDRG1/Cap43 overexpression in a HCC cell line, KIM-1, in vivo

We subsequently examined whether the overexpression of NDRG1/Cap43 could modulate tumor growth in mice under xenograft assay systems. The tumor growth of KIM-1/Cap43 showed markedly reduced rates as compared with its mock-transfected lines, KIM-1/Mock and (Fig. 4A). H&E analysis showed no apparent morphological differences in tumor samples 7 weeks after inoculation between cell lines with and without NDRG1/Cap43 (Fig. 4B). NDRG1/Cap43 expression in cancer cells was confirmed immunohistochemically in xenografts of KIM-1/Cap43 and HAK-1B/Cap43 cells (Fig. 4B). By contrast, there was almost no expression of NDRG1/Cap43 in xenografts of KIM-1/Mock and HAK-1B/Cap43. We next compared G_0/G_1-specific cell cycle related markers, p21 and CDK4, and also a representative proliferation marker, Ki-67 in mouse xenografts by immunohistochemical analysis. The rate of p21 positive cells in KIM-1/Cap43 tumor was significantly ($P < 0.05$) higher than in those of KIM-1/Mock tumor (Fig. 4C). On the other hand, the rate of CDK4 positive cells in xenograft of KIM-1/Cap43 was significantly ($P < 0.05$) lower than in that of KIM-1/Mock. The Ki-67 labeling index was significantly lower in KIM-1/Cap43 tumor than in the control KIM-1/Mock tumor (Fig. 4C). We did not observe any apparent difference in tumor microvascular density between KIM-1/Mock and KIM-1/Cap43 tumor (data not shown).

3.4. Tumor growth suppression by NDRG1/Cap43 overexpression in another HCC cell line, HAK-1B

To further confirm the suppressive effect of NDRG1/Cap43 overexpression on tumor growth by HCC cells *in vivo*, we established NDRG1/Cap43 overexpressing cell line from a different HCC cell line. Of two HCC cell lines, HAK-1A and HAK-1B, HAK-1A was derived from well differentiated type HCC and HAK-1B was from poorly differentiated type [22]. NDRG1/Cap43 is also a differentiation regulated protein. HAK-1A showed higher expression of NDRG1/Cap43 than HAK-1B (Fig. 5A). HAK-1B/Cap43 that was established by transfection of NDRG1/Cap43 cDNA into HAK-1B expressed a much higher expression of NDRG1/Cap43 than its parental counterpart HAK-1B/Mock (Fig. 5B). Western blot analysis demonstrated an increase in p21 and a decrease in CDK4 in HAK-1B/Cap43 cells in culture under full confluent condition as compared with its control counterpart (Fig. 5C). Tumor growth by HAK-1B/Cap43 demonstrated marked reduction as compared with HAK-1B/Mock (Fig. 5D). In a different HCC cell line, NDRG1/Cap43 overexpression thus induced a suppressive effect on the tumor growth.

4. Discussion

In our present study, we established hepatic cancer KIM-1/Cap43 cell line expressing stably higher amounts of NDRG1/Cap43, and observed the following characteristics. (1) The growth rate of KIM-1/Cap43 was significantly slower *in vitro* compared with that of the control KIM-1/Mock, and tumor growth in the xenograft model system was markedly suppressed by NDGR1/Cap43 overexpression; (2) Expression of G_0/G_1-specific p21 was up-regulated in confluent culture condition *in vitro* and in the tumor of mouse xenograft by NDRG1/Cap43 overexpression; (3) Treatment with mimosine, an inhibitor of G_1/G_0, also increased the expression of NDRG1/Cap43 together with increased expression of p21 and decreased expression of CDK4; (4) Immunohistochemical analysis showed much less expression of CDK4 in cancer cells of KIM-1/Cap43 tumor than those of KIM-1/Mock tumor, and KIM-1/Mock tumor showed the appearance of more Ki-67-positive cancer cells than KIM-1/Cap43 tumor. Taking these findings together, the marked suppression of tumor growth by NDRG1/Cap43 might be due to the activation or the loss of cell cycle or proliferation-promoting biomarkers, such as p21, CDK4 and Ki-67, respectively. Furthermore, we established another NDRG1/Cap43 overexpressing cell line

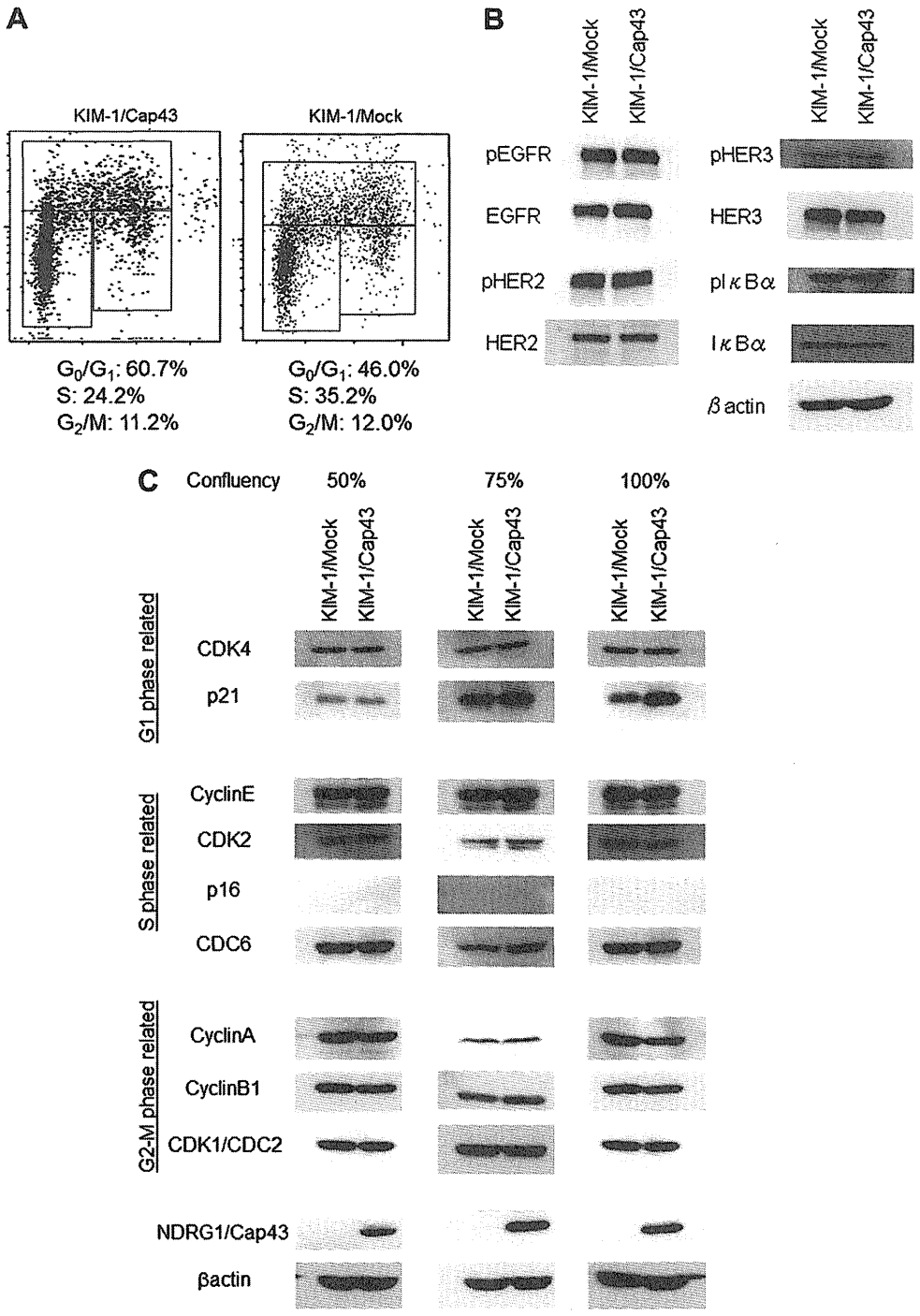

Fig. 2. Effect of NDRG1/Cap43 on cell cycle and cell cycle regulators. (A) KIM-1/Cap43 and KIM-1/Mock were cultured in serum-free culture medium for 24 h. After culturing in medium containing 10% FBS for 12 h, cells were subjected to cell cycle analysis. G_0/G_1 phase cell cycle arrest was observed in NDRG1/Cap43 transfectant, KIM-1/Cap43, as compared with mock transfectant, KIM-1/Mock. (B) There was no apparent difference in various growth factor receptors and their phosphorylated proteins. Expression of IκBα and plκBα was reduced in KIM-1/Cap43 as compared to KIM-1/Mock. (C) Expression of several cell cycle regulators was examined. Induction of p21 was observed in KIM-1/Cap43 under confluent culture condition. The other cell cycle regulators were not different despite NDRG1/Cap43 expression.

using HAK-1B. A stable transfectant of NDRG1/Cap43, HAK-1B/Cap43 showed p21 induction accompanied by CDK4 reduction in confluent culture condition *in vitro*. NDRG1/Cap43 overexpression also resulted in suppression of tumor growth of HAK-1B, similar to the suppressive effect in KIM-1. Considering these findings together, we favor the idea that NDRG1/Cap43 functions as tumor growth suppression in HCC.

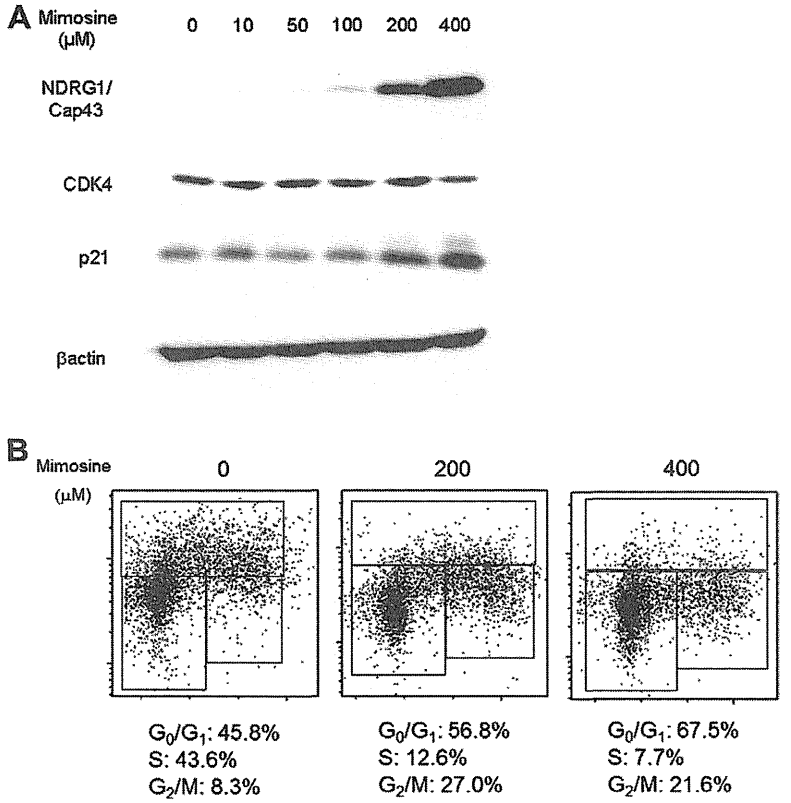

Fig. 3. Mimosine treatment in culture cell. (A) Dose-dependent study with different concentrations of mimosine for 24 h. NDRG1/Cap43 was induced when treated with 200 μM and 400 μM of mimosine. Mimosine induced p21 expression at 200 μM and 400 μM and inhibited CDK4 expression at 400 μM. (B) Cell cycle analysis with or without mimosine. Cell cycle was arrested at the G_0/G_1 phase when treated with 200 μM and 400 μM of mimosine.

NDRG1/Cap43 showed growth suppression in HCC cells *in vitro* and *in vivo*, consistent with the findings of previous studies [14,23]. Cell-cell contact often induces cell cycle arrest at the G_0/G_1 phase, through nuclear localization of p21 [24,25]. Suppressive expression of p21 was also observed in KIM-1/Mock tumor with increased expression of CDK4 as compared with KIM-1/Cap43 tumor. Expression of p21 was enhanced in KIM-1/Cap43 *in vitro* under the confluent culture condition. NDRG1/Cap43 may thus induce cell cycle arrest of HCC cells at G_0/G_1 through up-regulation of this key cell cycle regulator, p21. Several studies have documented the intranuclear p21 in senescent hepatocytes in many forms of chronic liver disease [26–30]. However, how p21 could be associated with the cell cycle growth arrest by hepatocyte remains unclear. Further study is required to determine whether NDRG1/Cap43 is involved in senescence of hepatocytes in liver diseases.

CDK4 is a cyclin dependent kinase composed of approximately 20 species. Microarray analysis of HCC revealed the patient population with low survival had high expression of CDK4 suggesting that CDK4 is a prognosis biomarker for HCC [31]. In the early G_1 phase, CDK4 and/or CDK6 are activated by D-type cyclin and initiate phosphorylation of retinoblastoma protein family [32,33]. This leads to the release of E2F transcription factors and results in the activation and transcription of E2F responsive genes required for cell cycle progression [34,35]. Cell cycle arrest at the G_0/G_1 phase is mediated by Cip/Kip families and/or Ink4a activation, followed by CDKs reduction [36]. Although the expression of p21 was up-regulated under confluent culture condition, that of CDK4 was not apparently changed in our present study (Fig. 2C). By contrast, increased expression of p21 and reduced expression of CDK4 were observed by mimosine treatment *in vitro*, and also in mouse xenograft tumor (Figs. 3A and 4C). Independent studies have reported that treatment with mimosine, a specific G_1 blocker resulted in marked up-regulation of NDRG1/Cap43 and down-regulation of CDK4 in other human cancer cell line in culture [37,38]. In HCC cells, treatment of mimosine at 200 μM and 400 μM induced expression of p21 and NDRG1/Cap43 while expression of CDK4 was decreased only when treated with 400 μM of mimosine (Fig. 3A). Induction of a certain amount of p21 by NDRG1/Cap43 might be a prerequisite for down regulation for CDK4. Since NDRG1/Cap43 expression is often up-regulated at the G_1 and G_2/M-phase but down-regulated in the S-phase of cancer cells [4], NDRG1/Cap43 may play a critical role in G_0/G_1 arrest possibly through altered expression of p21 and CDK4.

Ki-67 is a representative proliferation marker of tumor cells. Ki-67 expression is found throughout the cell cycle in the G_1, S and G_2/M phase and absent in the G_0 phase. In HCC, a high Ki-67 index was also associated with high histological grade, vascular invasion and advanced tumor

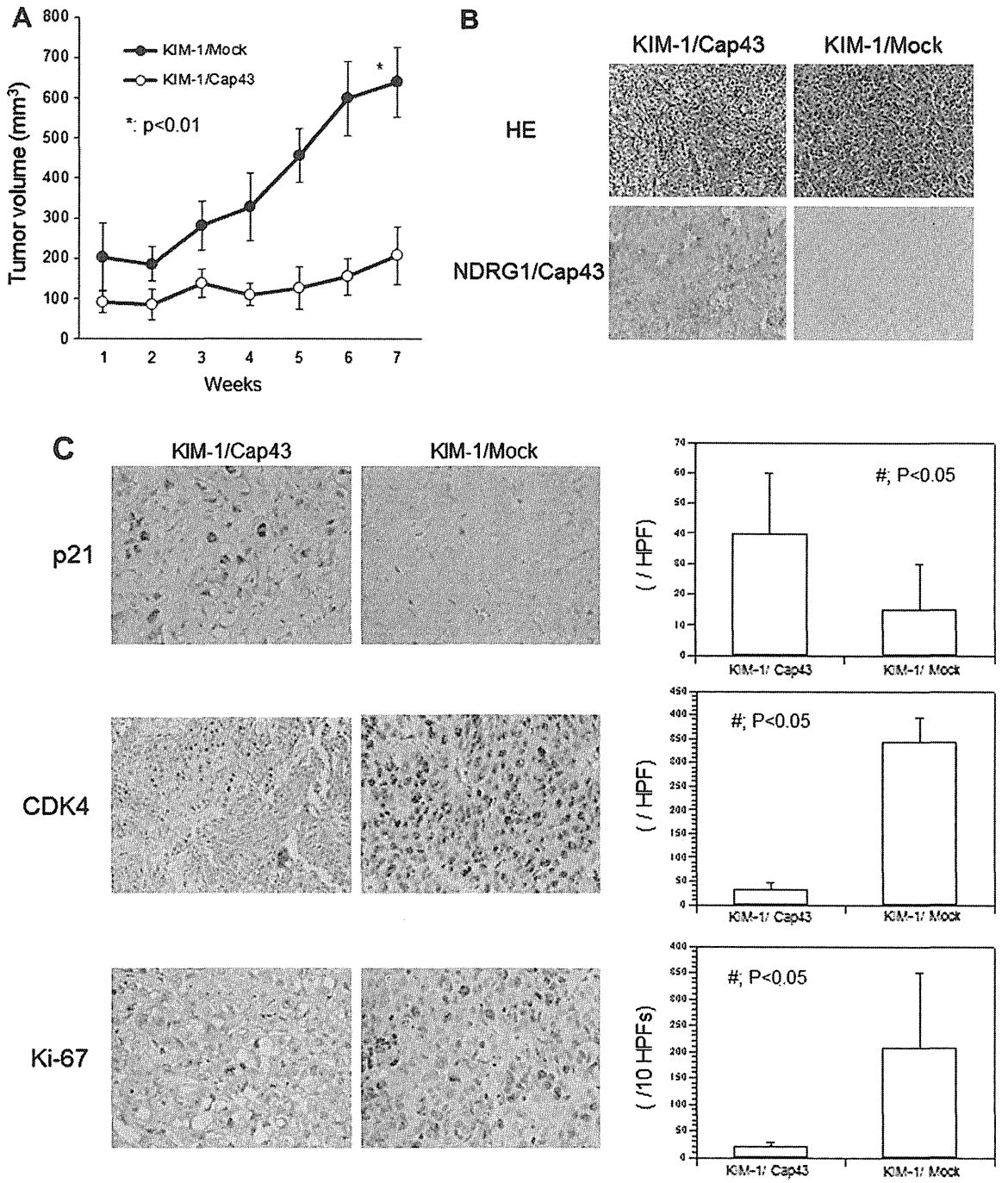

Fig. 4. Comparison of tumor growth and morphological findings between NDRG1/Cap43 and mock transfectants *in vivo*. (A) Tumor volumes were measured every week after tumor implantation. Tumor growth of KIM-1/Cap43 showed markedly reduced rates as compared with its mock-transfected line, KIM-1/Mock ($n = 6$ mice each). (B) No morphological differences were observed between NDRG1/Cap43 and mock transfectants. NDRG1/Cap43 expression was confirmed in the xenograft of NDRG1/Cap43 transfectant (magnification 200×). (C) Immunohistochemical staining of p21, CDK4 and ki-67 in mouse xenograft. The expression of all cell cycle regulators examined here was located in nucleus. The number of p21 positive cells was significantly higher in the tumor of KIM-1/Cap43 ($P < 0.05$). The number of CDK4 positive cells was significantly lower in the tumor of KIM-1/Cap43 ($P < 0.05$). Ki-67 expression was significantly lower in the tumor of KIM-1/Cap43 ($P < 0.05$) (magnification 200×).

stage [39]. In our xenograft model, high Ki-67 expression was observed in tumor without NDRG1/Cap43 expression compared with tumor generated from NDRG1/Cap43 expression, suggesting that the great number of tumor cells with NDRG1/Cap43 expression tends to be in the G_0 (or G_0/G_1) phase. Taken together, NDRG1/Cap43 might

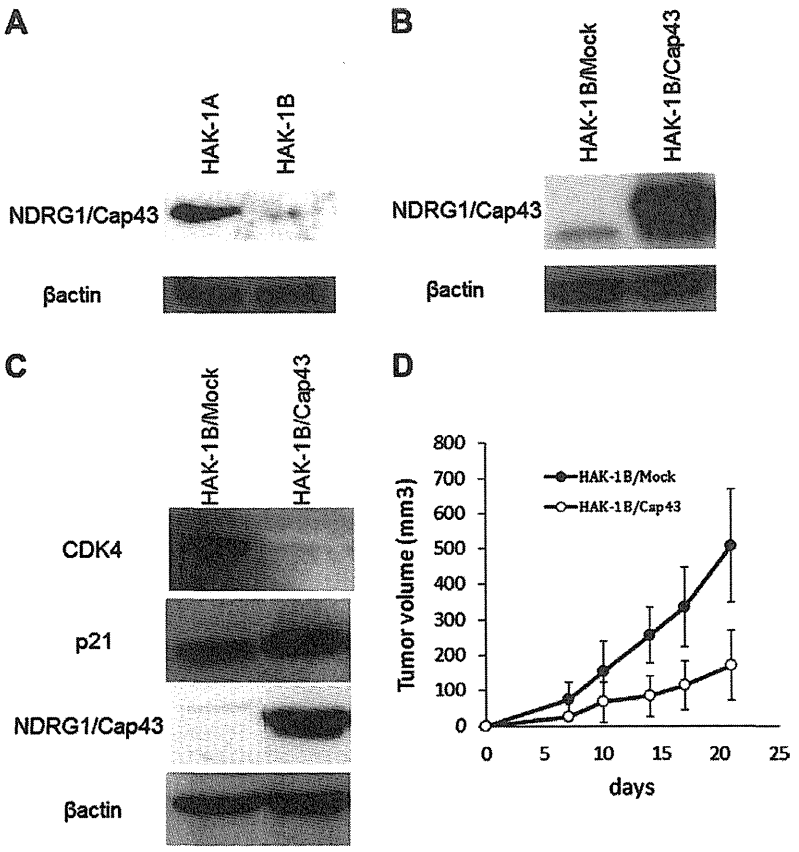

Fig. 5. (A) Expression of NDRG1/Cap43 in HAK-1A and HAK-1B examined by Western blot analysis. HAK-1A had apparent NDRG1/Cap43 expression, while HAK-1B had very low NDRG1/Cap43 expression. (B) Expression of NDRG1/Cap43 in HAK-1B/Cap43 and lack of NDRG1/Cap43 expression in HAK-1B/Mock were determined by Western blot analysis. (C) Induction of p21 and reduction of CDK4 were observed in HAK-1B/Cap43 under confluent culture condition. (D) Comparison of tumor growth between NDRG1/Cap43 and mock transfectants *in vivo*. Tumor volumes were measured every 3 days. Tumor growth of HAK-1B/Cap43 showed markedly reduced rates as compared with its mock transfected line, HAK-1B/Mock ($n = 4$ mice each).

attenuate activation of p21, leading to decreased expression of CDK4, resulting in cell cycle arrest at the G_0/G_1 phase (Fig. 6).

On the other hand, our previous study demonstrated the suppressive effect of NDRG1/Cap43 on tumor growth by pancreas cancer cells [14]. As the underlying mechanism for tumor suppressive effect, NDRG1/Cap43 overexpression was accompanied by reduced expression of IκBα and pIκBα in pancreas cancer cells [23,40]. Consistent with these previous reports, our present study demonstrated reduced expression of both IκBα and pIκBα in KIM-1/Cap43 as compared with KIM-1/Mock. NDRG1/Cap43-induced tumor suppressive effect might be in part due to the decreased NF-κB signaling pathway in HCC cells.

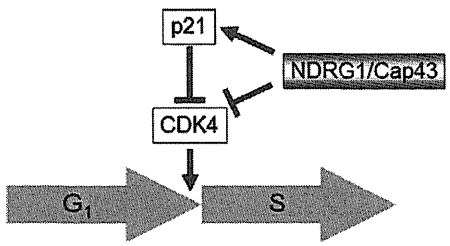

Fig. 6. Our hypothetical model of how NDRG1/Cap43 regulates cell cycle arrest at the G_0/G_1 phase. NDRG1/Cap43 attenuated activation of p21, leading to decreased expression of CDK4. NDRG1/Cap43 might thus mediate cell cycle arrest at the G_0/G_1 phase.

Based on our present study, NDRG1/Cap43-induced down-regulation of cell growth-related genes may be preferably involved in the tumor growth suppression by NDRG1/Cap43 overexpression. On the other hand, two research groups including ours have reported that NDRG1/Cap43 was related to the aggressive behavior and poor prognosis in human HCC tissues [18,19]. Yan and colleagues noted that NDRG1/Cap43 had a promoting effect on the proliferation and invasion of HCC cell lines [20]. Although there was no mechanism underlying why NDRG1/Cap43 promotes growth and malignancy by HCC cells in these studies, these results contrast with our present findings that NDRG1/Cap43 had an inhibitory effect on tumor growth of the HCC cell line. The reason for the discrepancy among these studies remains unknown at present, and further more precise studies are required to clarify the discrepancy.

In conclusion, this study has shown that NDRG1/Cap43 induces G_0/G_1-phase cell cycle arrest in HCC cell lines, and thereby exhibits an inhibitory effect on tumor growth,

suggesting that cell cycle regulators such as p21 and CDK4 might be involved in NDRG1/Cap43-induced cell cycle arrest. NDRG1/Cap43 might be a novel biomarker for developing an anticancer therapeutic strategy for HCC.

Conflicts of interest

None declared.

Acknowledgements

We thank Ms. Akemi Fujiyosi, Sachiyo Maeda and Akiko Tanaka for their excellent technical assistance and Ms. Yasuko Higuchi and Ms. Hisae Yoshioka for manuscript preparation.

References

[1] Y. Tanaka, K. Hanada, M. Mizokami, A.E. Yeo, J.W. Shih, T. Gojobori, H.J. Alter, A comparison of the molecular clock of hepatitis C virus in the United States and Japan predicts that hepatocellular carcinoma incidence in the United States will increase over the next two decades, Proc. Natl. Acad. Sci. USA 99 (2002) 15584–15589.
[2] M. Kudo, Early detection and curative treatment of early-stage hepatocellular carcinoma, Clin. Gastroenterol. Hepatol. 3 (2005) 144–148.
[3] K. Kokame, H. Kato, T. Miyata, Homocysteine-respondent genes in vascular endothelial cells identified by differential display analysis: GRP78/BiP and novel genes, J. Biol. Chem. 271 (1996) 29659–29665.
[4] S.K. Kurdistani, P. Arizti, C.L. Reimer, M.M. Sugrue, S.A. Aaronson, S.W. Lee, Inhibition of tumor cell growth by RTP/rit42 and its responsiveness to p53 and DNA damage, Cancer Res. 58 (1998) 4439–4444.
[5] D. Zhou, K. Salnikow, M. Costa, Cap43, a novel gene specifically induced by Ni2+ compounds, Cancer Res. 58 (1998) 2182–2189.
[6] A. Shimono, T. Okuda, H. Kondoh, N-myc-dependent repression of ndr1, a gene identified by direct subtraction of whole mouse embryo cDNAs between wild type and N-myc mutant, Mech. Dev. 83 (1999) 39–52.
[7] K. Masuda, M. Ono, M. Okamoto, W. Morikawa, M. Otsubo, T. Migita, M. Tsuneyoshi, H. Okuda, T. Shuin, S. Naito, M. Kuwano, Downregulation of Cap43 gene by von Hippel-Lindau tumor suppressor protein in human renal cancer cells, Int. J. Cancer 105 (2003) 803–810.
[8] E. Gomez-Casero, M. Navarro, M.L. Rodriguez-Puebla, F. Larcher, J.M. Paramio, C.J. Conti, J.L. Jorcano, Regulation of the differentiation-related gene Drg-1 during mouse skin carcinogenesis, Mol. Carcinogen. 32 (2001) 100–109.
[9] T. Okuda, Y. Higashi, K. Kokame, C. Tanaka, H. Kondoh, T. Miyata, Ndrg1-deficient mice exhibit a progressive demyelinating disorder of peripheral nerves, Mol. Cell Biol. 24 (2004) 3949–3956.
[10] B. Chen, D.M. Nelson, Y. Sadovsky, N-myc down-regulated gene 1 modulates the response of term human trophoblasts to hypoxic injury, J. Biol. Chem. 281 (2006) 2764–2772.
[11] P. Lachat, P. Shaw, S. Gebhard, N. van Belzen, P. Chaubert, F.T. Bosman, Expression of NDRG1, a differentiation-related gene, in human tissue, Histochem. Cell Biol. 118 (2002) 399–408.
[12] S. Bandyopadhyay, S.K. Pai, S.C. Gross, S. Hirota, S. Hosobe, K. Miura, K. Saito, T. Commes, S. Hayashi, M. Watabe, K. Watabe, The Drg-1 gene suppresses tumor metastasis in prostate cancer, Cancer Res. 63 (2003) 1731–1736.
[13] S. Bandyopadhyay, S.K. Pai, S. Hirota, S. Hosobe, Y. Takano, K. Saito, D. Piquemal, T. Commes, M. Watabe, S.C. Gross, Y. Wang, S. Ran, K. Watabe, Role of the putative tumor metastasis suppressor gene Drg-1 in breast cancer progression, Oncogene 23 (2004) 5675–5681.
[14] Y. Maruyama, M. Ono, A. Kawahara, T. Yokoyama, Y. Basaki, M. Kage, S. Aoyagi, H. Kinoshita, M. Kuwano, Tumor growth suppression in pancreatic cancer by a putative metastasis suppressor gene Cap43/NDRG1/Drg-1 through modulation of angiogenesis, Cancer Res. 66 (2006) 6233–6242.
[15] R.J. Guan, H.L. Ford, Y. Fu, Y. Li, L.M. Shaw, A.B. Pardee, Drg-1 as a differentiation-related, putative metastatic suppressor gene in human colon cancer, Cancer Res. 60 (2000) 749–755.
[16] M.A. Shah, N. Kemeny, A. Hummer, M. Drobnjak, M. Motwani, C. Cordon-Cardo, M. Gonen, G.K. Schwartz, Drg1 expression in 131 colorectal liver metastases: correlation with clinical variables and patient outcomes, Clin. Cancer Res. 11 (2005) 3296–3302.
[17] S. Nishio, K. Ushijima, N. Tsuda, S. Takemoto, K. Kawano, T. Yamaguchi, N. Nishida, T. Kakuma, H. Tsuda, T. Kasamatsu, Y. Sasajima, M. Kage, M. Kuwano, T. Kamura, Cap43/NDRG1/Drg-1 is a molecular target for angiogenesis and a prognostic indicator in cervical adenocarcinoma, Cancer Lett. 264 (2008) 36–43.
[18] M.S. Chua, H. Sun, S.T. Cheung, V. Mason, J. Higgins, D.T. Ross, S.T. Fan, S. So, Overexpression of NDRG1 is an indicator of poor prognosis in hepatocellular carcinoma, Mod. Pathol. 20 (2007) 76–83.
[19] J. Akiba, S. Ogasawara, A. Kawahara, N. Nishida, S. Sanada, F. Moriya, M. Kuwano, O. Nakashima, H. Yano, N-myc downstream regulated gene 1 (NDRG1)/Cap43 enhances portal vein invasion and intrahepatic metastasis in human hepatocellular carcinoma, Oncol. Rep. 20 (2008) 1329–1335.
[20] X. Yan, M.S. Chua, H. Sun, S. So, N-Myc down-regulated gene 1 mediates proliferation, invasion, and apoptosis of hepatocellular carcinoma cells, Cancer Lett. 262 (2008) 133–142.
[21] A. Kawahara, K. Azuma, S. Hattori, K. Nakashima, Y. Basaki, J. Akiba, S. Takamori, H. Aizawa, T. Yanagawa, H. Izumi, K. Kohno, S. Kono, M. Kage, M. Kuwano, M. Ono, The close correlation between 8-hydroxy-2'-deoxyguanosine and epidermal growth factor receptor activating mutation in non-small cell lung cancer, Hum. Pathol. 41 (2010) 51–959.
[22] H. Yano, A. Iemura, K. Fukuda, H. Mizoguchi, M. Haramaki, M. Kojiro, Establishment of two distinct human hepatocellular carcinoma cell lines from a single nodule showing clonal dedifferentiation of cancer cells, Hepatology 18 (1993) 320–327.
[23] F. Hosoi, H. Izumi, A. Kawahara, Y. Murakami, H. Kinoshita, M. Kage, K. Nishio, K. Kohno, M. Kuwano, M. Ono, N-myc downstream regulated gene 1/Cap43 suppresses tumor growth and angiogenesis of pancreatic cancer through attenuation of inhibitor of kappaB kinase beta expression, Cancer Res. 69 (2009) 983–4991.
[24] M. Küppers, C. Ittrich, D. Faust, C. Dietrich, The transcriptional programme of contact-inhibition, J. Cell. Biochem. 110 (2010) 234–1243.
[25] M.G. Ritt, J. Mayor, J. Wojcieszyn, R. Smith, C.L. Barton, J.F. Modiano, Sustained nuclear localization of p21/WAF-1 upon growth arrest induced by contact inhibition, Cancer Lett. 158 (2000) 73–84.
[26] V. Paradis, N. Youssef, D. Dargère, N. Ba, F. Bonvoust, J. Deschatrette, P. Bedossa, Replicative senescence in normal liver, chronic hepatitis C, and hepatocellular carcinomas, Hum. Pathol. 32 (2001) 327–332.
[27] J.G. Lunz 3rd, H. Tsuji, I. Nozaki, N. Murase, A.J. Demetris, An inhibitor of cyclin-dependent kinase, stress-induced p21Waf-1/Cip-1, mediates hepatocyte mito-inhibition during the evolution of cirrhosis, Hepatology 41 (2006) 262–1271.
[28] H. Wagayama, K. Shiraki, T. Yamanaka, K. Sugimoto, T. Ito, K. Fujisawa, K. Takase, T. Nakano, p21WAF1/CTP1 expression and hepatitis virus type, Dig. Dis. Sci. 46 (2001) 074–2079.
[29] S.U. Wiemann, A. Satyanarayàna, M. Tsahuridu, H.L. Tillmann, L. Zender, J. Klempnauer, P. Flemming, S. Franco, M.A. Blasco, M.P. Manns, K.L. Rudolph, Hepatocyte telomere shortening and senescence are general markers of human liver cirrhosis, FASEB J. 16 (2002) 35–942.
[30] A. Marshall, S. Rushbrook, S.E. Davies, L.S. Morris, I.S. Scott, S.L. Vowler, N. Coleman, G. Alexander, Relation between hepatocyte G1 arrest, impaired hepatic regeneration, and fibrosis in chronic hepatitis C virus infection, Gastroenterology 128 (2005) 33–42.
[31] J.S. Lee, I.S. Chu, J. Heo, D.F. Calvisi, Z. Sun, T. Roskams, A. Durnez, A.J. Demetris, S.S. Thorgeirsson, Classification and prediction of survival in hepatocellular carcinoma by gene expression profiling, Hepatology 40 (2004) 667–676.
[32] C.J. Sherr, J.M. Roberts, CDK inhibitors: positive and negative regulators of G1-phase progression, Genes Dev. 13 (1999) 1501–1512.
[33] C.J. Sherr, J.M. Roberts, Living with or without cyclins and cyclin-dependent kinases, Genes Dev. 18 (2004) 2699–2711.
[34] R.A. Weinberg, The retinoblastoma protein and cell cycle control, Cell 81 (1995) 323–330.
[35] N. Dyson, The regulation of E2F by pRB-family proteins, Genes Dev. 12 (1998) 2245–2262.
[36] T. Abbas, A. Dutta, p21 in cancer: intricate networks and multiple activities, Nat. Rev. Cancer 9 (2009) 00–414.
[37] Z. Dong, R.J. Arnold, Y. Yang, M.H. Park, P. Hrncirova, Y. Mechref, M.V. Novotny, J.T. Zhang, Modulation of differentiation-related gene 1

expression by cell cycle blocker mimosine, revealed by proteomic analysis, Mol. Cell Proteomics 4 (2005) 993–1001.
[38] K.S. Kulp, S.L. Green, P.R. Vulliet, Iron deprivation inhibits cyclin-dependent kinase activity and decreases cyclin D/CDK4 protein levels in asynchronous MDA-MB-453 human breast cancer cells, Exp. Cell Res. 229 (1996) 0–68.
[39] E. Kitamura, E. Hatano, T. Higashi, N. Masato, S. Seo, Y. Nakamoto, K. Yamanaka, H. Nagata, K. Taura, K. Yasuchika, T. Nitta, S. Uemoto, Proliferative activity in hepatocellular carcinoma is closely correlated with glucose metabolism but not angiogenesis, J. Hepatol. 17 (2011). Epub ahead of print.
[40] Y. Murakami, F. Hosoi, H. Izumi, Y. Maruyama, H. Ureshino, K. Watari, K. Kohno, M. Kuwano, M. One, Identification of sites subjected to serine/threonine phosphorylation by SGK1 affecting N-myc downstream-regulated gene 1 (NDRG1)/Cap43-dependent suppression of angionenic CXC chemokine expression in human pancreatic cancer cells, Biochem. Biophys. Res. Commun. 396 (2010) 376–381.

NEOPLASIA
www.neoplasia.com

Volume 13 Number 3 March 2011 pp. 187–197 187

Metronomic S-1 Chemotherapy and Vandetanib: An Efficacious and Nontoxic Treatment for Hepatocellular Carcinoma[1]

Hideki Iwamoto*,†, Takuji Tsumura*,†, Toru Nakamura*,†, Osamu Hashimoto*,†, Kinya Inoue*,†, Junichi Kuroda*, Takashi Niizeki*, Reiichiro Kuwahara*, Mitsuhiko Abe*, Hironori Koga*, Hirohisa Yano‡, Robert S. Kerbel§, Takato Ueno*,† and Michio Sata*

*Division of Gastroenterology, Department of Medicine, Kurume University School of Medicine, Kurume, Japan; †Research Center for Innovative Cancer Therapy, Kurume University School of Medicine, Kurume, Japan; ‡Department of Pathology, Kurume University School of Medicine, Kurume, Japan; §Molecular and Cellular Biology Research Sunnybrook Health Sciences Centre, Toronto, Ontario, Canada

Abstract

BACKGROUND: Metronomic chemotherapy involves frequent, regular administration of cytotoxic drugs at nontoxic doses, usually without prolonged breaks. We investigated the therapeutic efficacies of metronomic S-1, an oral 5-fluorouracil prodrug, and vandetanib, an epidermal growth factor receptor and vascular endothelial growth factor (VEGF) receptor tyrosine kinase inhibitor, in models of hepatocellular carcinoma (HCC). *METHODS:* We compared anti-HCC effects and toxicity in the six treatment groups: control (untreated), maximum tolerated dose (MTD) S-1, metronomic S-1, vandetanib, MTD S-1 with vandetanib, and metronomic S-1 with vandetanib. Tumor microvessel density (MVD) and tumor apoptosis were evaluated by immunohistochemistry. The expression of VEGF and thrombospondin-1, an endogenous inhibitor of angiogenesis, was analyzed by Western blot. *RESULTS:* Metronomic S-1 significantly inhibited tumor growth, which was enhanced by combination with vandetanib. With respect to toxicities, MTD S-1 caused severe body weight loss and myelosuppression, whereas metronomic S-1 did not cause any overt toxicities. Moreover, metronomic S-1 or metronomic S-1 with vandetanib prolonged survival, the latter treatment providing the greatest benefit. Metronomic S-1 and metronomic S-1 with vandetanib decreased MVDs and increased apoptosis in tumor tissues. The expression of VEGF in tumor tissues was upregulated by vandetanib and metronomic S-1 with vandetanib, whereas the expression of thrombospondin-1 was upregulated by metronomic S-1 and metronomic S-1 with vandetanib. *CONCLUSION:* Metronomic S-1 with an antiangiogenic agent seems to be an effective and safe therapeutic strategy for HCC.

Neoplasia (2011) 13, 187–197

Introduction

Hepatocellular carcinoma (HCC) is the fifth most common solid tumor and the third leading cause of cancer-related deaths globally [1]. Although prognosis of early and intermediate stage HCC has improved owing to advances in treatments, there are few proven effective systemic therapies for advanced HCC [2]. In particular, conventional chemotherapy using cytotoxic drugs for advanced HCC has not been shown to improve survival. Almost all cases of HCC occur in patients with chronic liver disorders, such as liver cirrhosis. Patients with liver cirrhosis have liver dysfunction and also pancytopenia. These pathologies

Abbreviations: HCC, hepatocellular carcinoma; MTD, maximum tolerated dose; MVD, microvessel density; VEGF, vascular endothelial growth factor; EGF, epidermal growth factor; TSP-1, thrombospondin-1; HUVEC, human umbilical vascular endothelial cell

Address all correspondence to: Hideki Iwamoto, MD, Division of Gastroenterology, Department of Medicine, Kurume University School of Medicine, 67 Asahi-Machi, Kurume-shi, Fukuoka-ken, 830-0011, Japan. E-mail: iwamoto_hideki@med.kurume-u.ac.jp

[1]All authors agreed to the submission of this article, and there is no conflict to disclose.

Received 18 August 2010; Revised 6 December 2010; Accepted 8 December 2010

DOI 10.1593/neo.101186

limit the use of conventional chemotherapy as a treatment strategy for HCC.

Conventional chemotherapy often involves pulsatile administration schedules using maximum tolerated doses (MTDs) of cytotoxic drugs. The long break periods between therapies not only allow recovery from various toxicities, especially myelosuppression, but also provide an opportunity, unfortunately, for the drug-treated tumors to recover as well [3]. In contrast, metronomic chemotherapy is given at frequent intervals using minimally or nontoxic doses without prolonged breaks. In several preclinical studies, such metronomic protocols have shown surprisingly effective antitumor effects, despite the reduced toxicity [4–6].

S-1 is an orally novel cytotoxic 5-flurouracil (5-FU) prodrug, which consists of tegafur and two biochemical modulators, 5-chloro-2,4-dihydroxypyridine and potassium oxonate [7]. 5-Chloro-2,4-dihydroxypyridine competitively inhibits dihydropyrimidine dehydrogenase approximately 180 times more effectively than uracil. Thus, S-1 gives rise to high concentrations of 5-FU in blood and tumor tissue for long-term periods since biochemical modulation [7,8]. A drug similar to S-1, namely, UFT, has been used successfully in metronomic preclinical studies [5]. Moreover, in the clinic it has been used successfully in randomized phase 3 trials in a metronomic fashion to treat in an adjuvant manner a variety of early stage cancers, after surgery, including non–small cell lung cancer [9] and breast cancer [10]. Because S-1 is thought to be more potent than UFT with respect to the effect of biochemical modulations, one might expect a stronger antitumor effect by using S-1 [7]. In this study, we describe a method of administering metronomic S-1 to treat HCC and compare it to conventional MTD S-1 chemotherapy, either alone or with an antiangiogenic drug.

Tyrosine kinase inhibitors such as sorafenib have proven activity in HCC patients and now represent one of the few effective systemic therapies for HCC [11]. Preclinical studies have also shown that the antitumor effect of metronomic chemotherapy can be significantly enhanced by combination with vascular endothelial growth factor (VEGF) pathway targeting agents [12,13]. In this study, we show here that metronomic S-1 might be a promising therapy to consider for concurrent daily combination with an oral antiangiogenic drug, in this case, vandetanib (ZD6474; AstraZeneca Pharmaceuticals, Macclesfield, UK). Vandetanib inhibits not only the catalytic function of VEGFR-2 but also EGF receptors (EGFRs), in contrast to sorafenib or sunitinib that do not affect EGFRs [14]. We evaluated the efficacies of vandetanib alone *in vivo* for HCC-bearing mice using various hepatoma cell lines that had different expressions of EGFR (submitted for publication). EGFR is known to contribute to 5-FU drug resistance, and 5-FU is the major metabolite of S-1 [15]. Therefore, there is a rationale for drug targeting of both EGF receptors and VEGF receptors along with metronomic chemotherapy, which was the purpose of this study. Thus, we investigated the efficacy of combining with each treatment schedule of S-1 and vandetanib using two HCC cell lines, which express low or high levels of EGFR, that is, KYN-2 and Huh-7, respectively. Overall, our results suggest that the combination treatment of metronomic S-1 plus vandetanib may be useful for the therapy of HCC.

Materials and Methods

Cell Lines and Culture

In human hepatoma cell lines, Huh-7 was originally purchased from CAMBREX Bio Science Walkersville, Inc (Walkersville, MD), and KYN-2 was provided by the Department of Pathology, Kurume University School of Medicine. Cells were maintained in Dulbecco modified Eagle medium (DMEM; Gibco Invitrogen Cell Culture Co, Auckland, New Zealand) supplemented with 10% fetal bovine serum (FBS).

Human umbilical vascular endothelial cells (HUVECs) were purchased from CAMBREX Bio Science Walkersville, Inc, and maintained with endothelial cell growth medium-2 (Clonetics, San Diego, CA) containing 5% FBS.

Animals and Drugs

Male 5-week-old nude mice (BALB/c *nu/nu*) were purchased from Kyudo KK (Fukuoka, Japan). All experiments were conducted in accordance with the National Institutes of Health guidelines for the Care and Use of Laboratory Animals.

5-FU was purchased from Kyowa Hakko Kogyo Co, Ltd (Tokyo, Japan). S-1 was provided by Taiho Pharmaceutical Co, Ltd (Tokyo, Japan). S-1 consists of a mixture of tegafur, gimeracil, and oteracil at molar ratio of 1:0.4:1 in 0.5% hydroxypropylmethylcellulose (HPMC) solutions. Vandetanib (ZD6474; Zactima) was provided by AstraZeneca Pharmaceuticals (Macclesfield, UK).

In Vitro *Cell Proliferation Assay*

As the tegafur component of S-1 is physiologically converted to 5-FU in the body, we evaluated the difference of antiproliferative effects *in vitro* of 5-FU using different schedules with both hepatoma cells and HUVECs. Approximately 1000 cells in 100 μl of DMEM containing 10% FBS was added to each well of 96-well plate. After incubation for 24 hours, the medium was exchanged to the serum-containing medium with various concentrations of 5-FU (0, 1, 10, 100, 500, 1000, 10,000 ng/ml). Each cell line was exposed to 5-FU for 5 days. To evaluate the antiproliferative effect of "MTD" *versus* "metronomic" chemotherapy, exchange of the medium containing 5-FU was performed using different schedules. For the metronomic schedule, the medium containing 5-FU was exchanged daily as described previously [16]. For the MTD schedule, the medium containing 5-FU was not changed. After incubation, cell proliferation was evaluated by a tetrazolium-based assay (Cell Count Reagent SF; Nakalai Tesque, Inc, Kyoto, Japan).

Determination of the Optimal Dose for S-1 Using Metronomic Chemotherapy

We determined the optimal metronomic dose of S-1 according to a previous report, which involved evaluating different doses of a chemotherapy drug both for antitumor effects and toxicity, with the aim of determining a dose that has minimal toxicity but retains good efficacy [17]. A total of 5×10^6 Huh-7 cells were injected into the flank regions of nude mice. Therapy with different doses of S-1 was initiated when the estimated tumor volume ($0.52 \times \text{length} \times \text{width}^2$) reached 150 to 200 mm^3. Mice received S-1 orally administrated by gavage with the following agents on a daily basis for 14 days: 1) HPMC as the control group; 2) S-1, 7.5 mg/kg per day; 3) S-1, 5.0 mg/kg per day; 4) S-1, 2.5 mg/kg per day; or 5) S-1, 1.0 mg/kg per day. Tumor-bearing mice were randomly divided into groups of 10 mice. The mice were killed at day 15 after start of treatment. The inhibition rate of tumor growth (IR %) was calculated as follows: IR % = (1 − mean RTV of treatment group / mean RTV of control group) × 100, where RTV indicates the relative tumor volume: tumor volume on killing / tumor volume on initial treatment. For comparison of the toxicity in each group, mouse body weights were measured every 3 days. Peripheral leukocyte count and hemoglobin (Hb) concentrations of these mice were also measured at day 15.

Tumor Growth and Toxicity Assessment in the Subcutaneous Tumor Transplant Model

We selected as the optimal metronomic dosage for S-1, 5.0 mg/kg per day based on our aforementioned study. We selected the MTD for S-1 15 mg/kg per day for 7 days, followed by a 7-day break period, based on previous published findings [6]. To compare the antitumor effect and toxicity caused by MTD or metronomic S-1, long-term experiments were performed using the Huh-7 subcutaneous transplant model. Mice were randomly divided to six groups: 1) HPMC as the control group; 2) MTD S-1, 15 mg/kg per day p.o. for 1 week, followed by a 1-week break period for a cumulative dose of 95 mg/kg; 3) metronomic S-1, 5 mg/kg per day p.o. for 2 weeks without any break period for a cumulative dose of 70 mg/kg; 4) vandetanib 25 mg/kg per day p.o. for 2 weeks; 5) MTD S-1 with vandetanib; or 6) metronomic S-1 with vandetanib. Each group consisted of 10 mice. It is important to note that the cumulative metronomic doses were distinctly less than the cumulative MTD. In other words, whereas the schedule used was "dose-dense," it was not "dose intense." The aforementioned schedules were performed in two cycles, 4 weeks in total. Estimated tumor volumes were measured every 3 days, and all mice were killed after 4 weeks of treatment. For comparison of the toxicity in each group, mouse body weights were measured every 3 days. Peripheral leukocyte count and hemoglobin (Hb) concentrations in these mice were also measured at sacrifice.

Tumor Growth and Survival Assessment in the Orthotopic Transplant Model

We also examined tumor growth using an orthotopic liver transplant model. The mice were implanted with 2×10^6 KYN-2 cells into the left lobe liver. Mice were randomly divided into six groups, as outlined above, and therapy was initiated 7 days after implantation of tumor cells. Each group consisted of 10 mice. The mice were killed at day 29 of initial treatment, and tumor volumes were evaluated.

In addition, a survival study was also performed using the KYN-2 orthotopic transplant model for the six groups as mentioned above. Each group consisted of 10 mice. In the group for survival observation, animals were killed according to (pre)clinical signs of weakness, for example, anorexia, or greater than 20% weight loss, and days of life were recorded from initial treatment.

Immunohistochemical Staining of CD31, PCNA, and TUNEL

The sections of all tumor tissues obtained from KYN-2 orthotopic transplant model were boiled for 30 minutes by high pH target retrieval solution (DAKO Japan, Kyoto, Japan) for antigen retrieval. The sections were incubated with rabbit anti–human CD31 antibody (diluted 1:300; Abcam, Inc, Tokyo, Japan) and rabbit anti–human PCNA antibody (diluted 1:250; Abcam, Inc) at 4°C overnight. Then the avidin-biotin procedures were subsequently performed using a Vectastatin ABC Kit (Vector Laboratories, Inc, Burlingame, CA). The sections were reacted with 0.005% H_2O_2–3,3′-diaminobenzidine at room temperature for 1 minute. For quantification of microvessel density (MVD), CD31-positive vessels were counted in randomly selected 30 areas per five tumors in each treatment group at 200-fold magnification.

The terminal deoxynucleotidyl transferase–mediated dUTP nick end labeling (TUNEL) method was performed for the evaluation of apoptosis in each of the treated tumor tissues. TUNEL labeling was performed using the ApopTag Kit (Chemicon, Temecula, CA) according to the manufacturer's instructions. The stained sections of tumors of each group were reviewed, and the apoptosis index, determined by TUNEL staining, was determined by counting at least 1000 cells in five randomly selected high-power fields (magnification, ×200).

Expression of Thrombospondin-1 and VEGF in Tumor Tissues

We examined the expression of VEGF and thrombospondin-1 (TSP-1) in treated tumor tissues using Western blot analysis. TSP-1 is a known endogenous antiangiogenic protein [18]. Five samples of each treatment group and control group were loaded in equal conditions, respectively. Thirty micrograms of protein was loaded onto a NuPAGE 4% to 12% Bis-Tris gel (Invitrogen, CA). Membranes were incubated with rabbit anti–TSP-1 antibody (1:350 dilution; Abcam, Inc) or rabbit anti-VEGF antibody (1:500 dilution; Abcam, Inc) at 4°C overnight. Equal protein loading was assessed by mouse anti–β-actin antibody (1:1000 dilution; Sigma, St Louis, MO). After incubation with HRP-conjugated anti–rabbit immunoglobulin G (1:10,000 dilution; GE Healthcare UK Ltd, Buckinghamshire, UK) or HRP-conjugated anti–mouse immunoglobulin G antibody (1:5000 dilution; GE Healthcare UK Ltd) for 1 hour, immunoreactive bands were stained by an enhanced chemiluminescence Western blot analysis system using LAS 4000 mini (Fujifilm, Tokyo, Japan) and were calculated with the amount of luminescence in each sample using multigauge software (Fujifilm). The relative amount of luminescence in each treatment group for the control group was expressed as [(treatment group VEGF or TSP-1 / treatment group β-actin) / (control group VEGF or TSP-1 / control group β-actin)] and compared with each group.

Statistical Analysis

All experimental data were expressed as mean ± SD. Differences between groups were examined for statistical significance using the Mann-Whitney *U* test, the Kruskal-Wallis test, and nonparametric analysis of variance. If the one-way analysis of variance was significant, differences between individual groups were estimated using the Fisher least significant difference test. Overall survival was estimated according to the Kaplan-Meier method and compared using the log-rank test. $P < .05$ was considered to be statistically significant.

Results

Comparison of Antiproliferative Effects of Metronomic versus MTD Type Chemotherapy In Vitro

The 50% inhibitory concentration (IC_{50}) levels of metronomic and MTD schedules of 5-FU, the major metabolite of S-1, for each cell line are shown in Table 1. The antiproliferative effects of 5-FU for each cell line were found to be dose-dependent (Figure 1, *A–C*). The IC_{50} levels for the MTD and metronomic schedule for Huh-7 cells were 3.84 and 0.77 μM, respectively (Figure 1*A*). The IC_{50}

Table 1. IC_{50} Levels of MTD and Metronomic Schedule in Hepatoma Cell Lines and Endothelial Cell.

	5-FU IC_{50} (μM)	
	MTD	Metronomic
Hepatoma cell lines		
Huh-7	3.84	0.77
KYN-2	7.69	3.84
Endothelial cell		
HUVECs	7.7	0.76

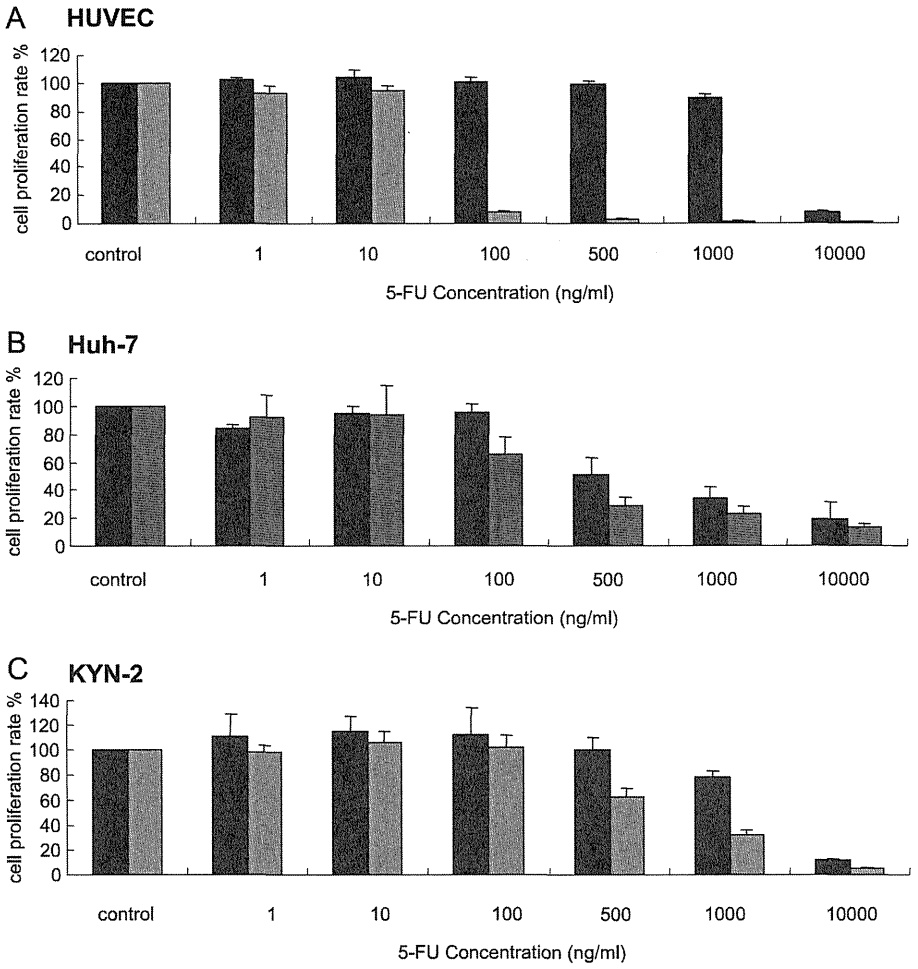

Figure 1. Inhibitory effect of metronomic chemotherapy for each cell line tested in a cell proliferation assay. To evaluate the antiproliferative effect of "MTD" and "metronomic" chemotherapy *in vitro*, exchange of the medium containing 5-FU was performed in different schedules. For the metronomic schedule, the medium containing 5-FU (0, 1, 10, 100, 500, 1000, and 10,000 ng/ml) was exchanged once a day. For the MTD schedule, the medium containing 5-FU was not changed. Data are shown as a ratio of the control and expressed as mean ± SD of 10 samples. *$P < .001$ compared with each schedule. Dark gray–shaded columns show MTD schedule, and light gray–shaded columns showed metronomic schedule. (A) HUVEC. HUVEC was cultured with 100 μl of endothelial cell growth medium-2 with 5% FBS containing 5-FU. (B) Huh-7. (C) KYN-2. Hepatoma cells were cultured with 100 μl of DMEM with 10% FBS containing 5-FU.

levels for KYN-2 were 7.69 and 3.84 μM, respectively. For the hepatoma cell lines, the metronomic schedule inhibited cell proliferation at approximately 1/2 to 1/4 concentrations of 5-FU compared with MTD schedule (Table 1). The metronomic schedule for HUVECs inhibited cell proliferation at apparently lower levels (IC_{50} levels, 0.76 μM) approximately 1/10 the concentration of 5-FU compared with MTD schedule (IC_{50} levels, 7.7 μM; Table 1).

Determination of the Optimal Dose of S-1 for Metronomic Chemotherapy In Vivo*: Maximum Tumor Growth Inhibition with Minimal Toxicity*

In the 7.5- and 5.0-mg/kg-per-day S-1 treatment groups, there were significant differences in suppression of tumor growth compared with the control group ($P < .05$; Figure 2*A*), and dosages lower than 2.5 mg/kg per day S-1 were not statistically effective compared with the control group. In addition, we evaluated body weight loss and myelosuppression toxicities associated with administration of S-1 (Figure 2, *B–D*). With respect to body weight loss, there was no significant difference between each group (Figure 2*B*). But only the 7.5-mg/kg-per-day group showed severe toxicity as determined by reductions in Hb concentration and leukocyte count ($P < .001$, compared with the control group; Figure 2, *C* and *D*). Therefore, we selected 5.0 mg/kg per day as the optimal metronomic dosage of S-1, which was used in all subsequent experiments.

Evaluation of the Antitumor Effect and Toxicity for Metronomic S-1 Chemotherapy in the Subcutaneous Transplant Tumor Model

In the assay for tumor growth, statistical differences were observed between the control group and all treatment groups (Figure 3*A*).

Metronomic S-1 potently inhibited tumor growth compared with MTD S-1 ($P < .01$). The mean tumor volumes were 4810.5 ± 1440.9 cm^3 in the control group, 3212.6 ± 1364.7 cm^3 in the MTD S-1 group, 1927.1 ± 652.9 cm^3 in the metronomic S-1 group, and 2331.4 ± 662.1 cm^3 in the vandetanib group, respectively. The mean tumor volumes in the MTD S-1 plus vandetanib group and metronomic S-1 plus vandetanib group were 2026.7 ± 1106.7 and 1383.7 ± 697.5 cm^3, respectively. The greatest inhibition of tumor growth was induced by the metronomic S-1 in combination with vandetanib (Figure 3*A*). In addition, we evaluated toxicity in each of Huh-7 subcutaneous tumor treatment groups (Figure 3, *B–D*). In leukocyte count, there were no significant differences in the groups (Figure 3*B*). In Hb concentration, the control group was 12.84 ± 1.82 g/dl, the MTD S-1 group was 9.77 ± 3.63 g/dl, the metronomic S-1 group was 11.73 ± 3.27 g/dl, and the vandetanib group was 12.34 ± 2.77 g/dl. For the combination treatments, the MTD S-1 plus vandetanib group was 8.24 ± 1.64 g/dl, and for the metronomic S-1 plus vandetanib group, it was 11.74 ± 1.55 g/dl (Figure 3*C*). With respect to rate of body weight loss, in the MTD S-1 monotherapy and MTD S-1 with vandetanib groups, the values observed were 10.48% ± 6.85% and 8.59% ± 5.02% reduction compared with the control group, respectively. Vandetanib, metronomic S-1, and the combination therapy resulted in 5.64% ± 4.23%, 3.04% ± 2.23%, and −0.51% ± 5.56% reduction compared with the control group, respectively (Figure 3*D*). Both the MTD S-1 and MTD S-1 plus vandetanib treatment groups experienced severe body weight loss and reduced Hb concentrations compared with the control group (Figure 3, *C* and *D*). In marked contrast, the metronomic S-1 monotherapy and metronomic S-1 with vandetanib groups did not manifest any overt toxicity (Figure 3, *B–D*).

Evaluation of Antitumor Efficacy Using Metronomic S-1 Chemotherapy in an Orthotopic Liver Transplant Model

For tumor volume assessments, all treatments except MTD S-1 monotherapy were effective compared with the control group (Figure 4*A*). Tumor volumes at sacrifice were 4186.0 ± 1128.0 cm^3 in the control group, 3259.0 ± 788.7 cm^3 in the MTD S-1 group, 1501.3 ± 1002.2 cm^3 in the metronomic S-1 group, and 1582.0 ± 354.9 cm^3 in the vandetanib group. There was a significant difference between metronomic S-1 and MTD S-1 in tumor growth inhibition ($P < .05$; Figure 4*A*). For the combination treatment groups, tumor volumes were 931.1 ± 331.7 cm^3 in the MTD S-1 plus vandetanib group and 875.0 ± 369.4 cm^3 in the metronomic S-1 plus vandetanib group. There was no significant difference between the metronomic S-1 plus vandetanib group and the MTD S-1 plus vandetanib group. However, the greatest inhibition of tumor growth was detected in the metronomic S-1 plus vandetanib treatment group ($P < .001$; Figure 4*A*).

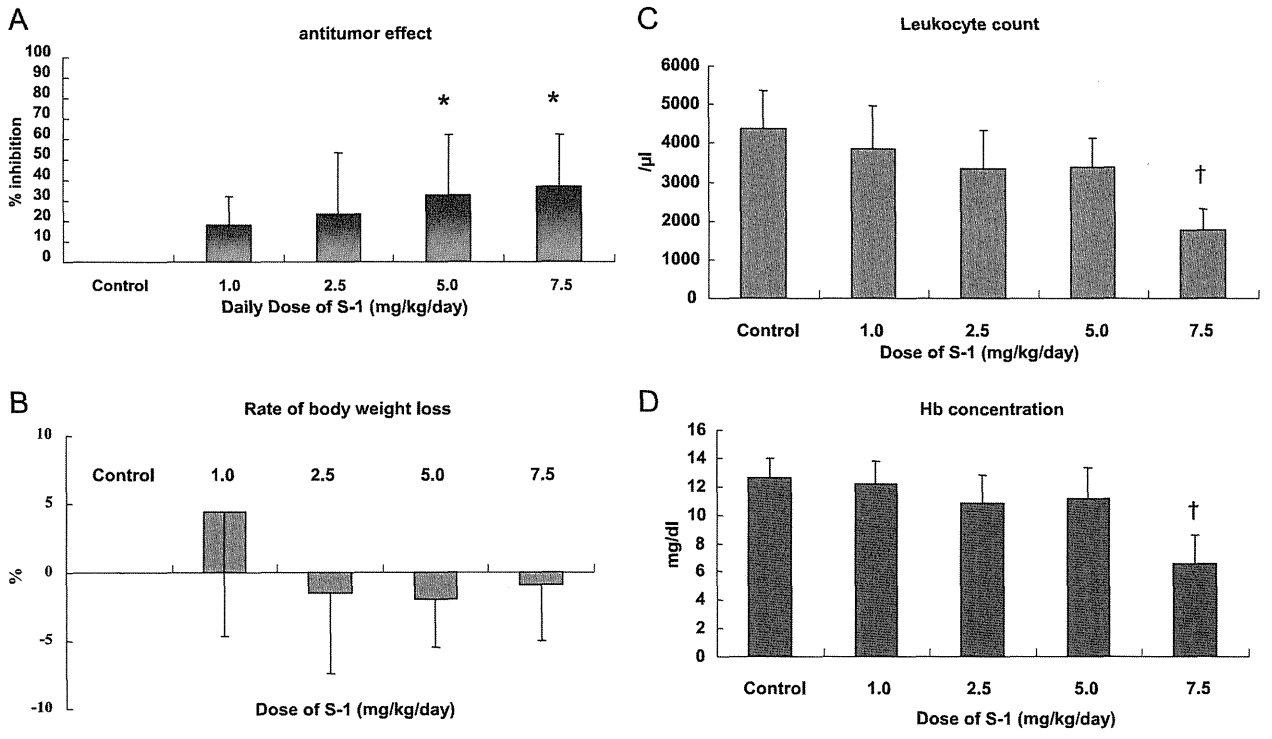

Figure 2. Determination of the optimal dose of S-1 in metronomic chemotherapy. Huh-7 subcutaneous tumor models were treated daily with either HPMC or different metronomic doses of S-1 (1.0, 2.5, 5.0, or 7.5 mg/kg per day) for 14 consecutive days. (A) Inhibition rates of tumor volumes (%) are expressed as mean ± SD ($n = 10$ per group). Dosages of 5.0 and 7.5 mg/kg per day S-1 groups statistically inhibited tumor growth compared with the control group (*$P < .05$). (B–D) Toxicity parameters are represented as mean ± SD. (B) Body weight (BW) changes on killing were calculated according to the following formula: BW change (%) = [(BW on sacrifice) − (BW on day 0)] × 100. (C) Hb concentration. (D) Leukocyte count. Each different dose of S-1 did not show body weight loss. However, the only 7.5-mg/kg-per-day S-1 group represented severe myelosuppression, such as decreased Hb concentration or leukocyte count. †$P < .001$ by compared with the control group.

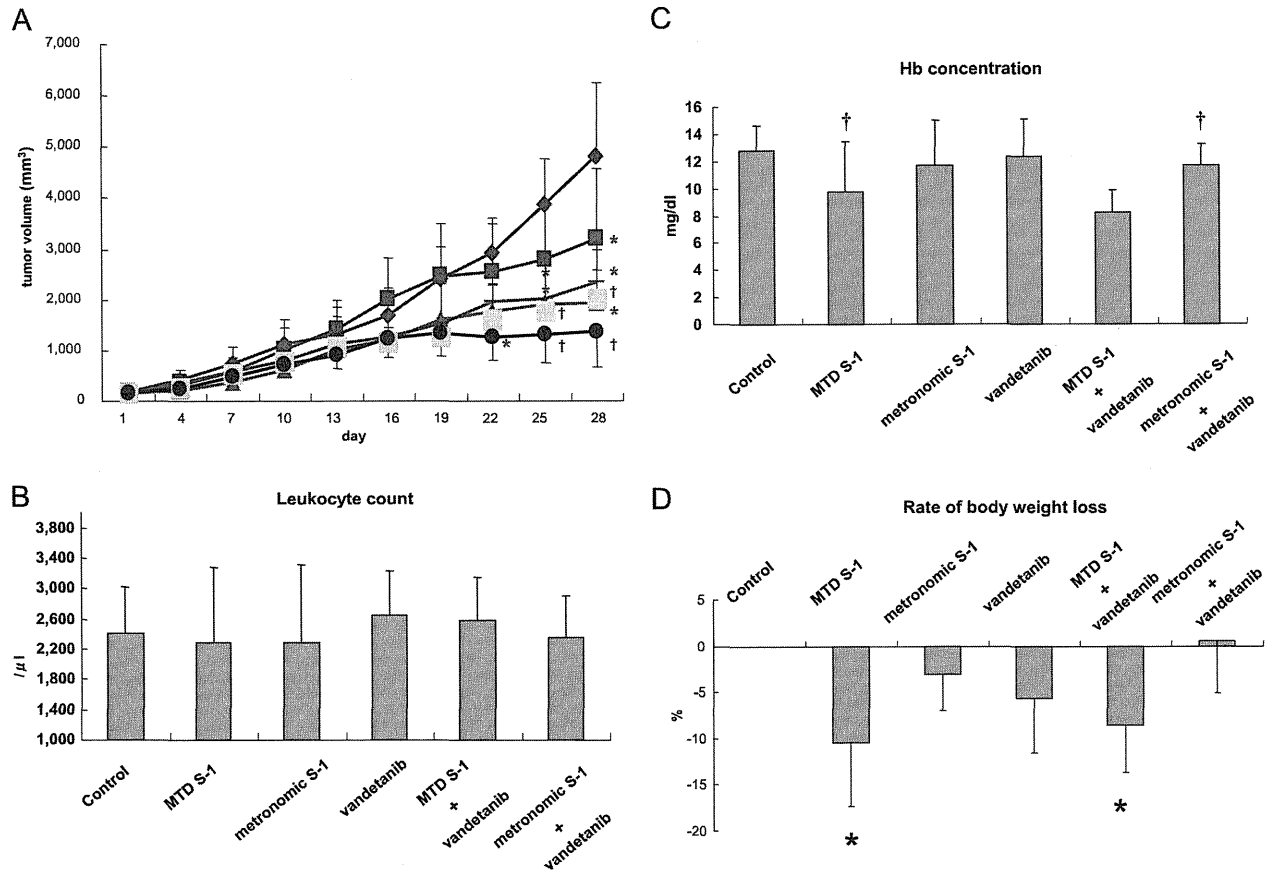

Figure 3. Therapeutic effects of metronomic S-1 chemotherapy in the Huh-7 subcutaneous tumor transplant model. (A) Tumor-bearing nude mice (n = 10 per group) were treated in the following six groups: 1) HPMC as the control group (blue); 2) MTD S-1 15 mg/kg per day for 1 week, followed by a 1-week break period (purple); 3) metronomic S-1 5 mg/kg per day for 2 weeks without break period (green); 4) vandetanib 25 mg/kg per day for 2 weeks (red); 5) MTD S-1 with vandetanib (yellow); or 6) metronomic S-1 with vandetanib (black). All treatments were performed for 4 weeks in total. Tumor volume changes are expressed as mean ± SD. All treatments showed efficacy compared with the control group (*P < .05), and the metronomic S-1 therapy was more effective than the MTD S-1 treatment. The metronomic S-1 with vandetanib significantly inhibited tumor growth compared with the control group (†P < .001). (B–D) Toxicity parameters are expressed as mean ± SD. (B) Hb concentration. (C) Leukocyte count. (D) Rate of body weight loss. MTD S-1 and the MTD S-1 with vandetanib showed severe body weight loss (*P < .01) and decreased Hb concentration (†P < .05) compared with the control group. Metronomic S-1 and the metronomic S-1 with vandetanib did not show any overt toxicities.

Evaluation of Survival Using Metronomic S-1 Chemotherapy in an Orthotopic Liver Transplant Model

The mean survival time in the control group was 28.9 ± 6.4 days. MTD S-1 did not prolong survival (mean survival time, 29.6 ± 3.9 days). In contrast, metronomic S-1 significantly prolonged survival (mean survival time, 34.3 ± 4.8 days). The mean survival time in the vandetanib group was 33.6 ± 5.0 days. MTD S-1 plus vandetanib treatment did not prolong survival times compared with vandetanib monotherapy (mean survival time, 37.6 ± 5.5 days). However, the metronomic S-1 plus vandetanib group provided the greatest prolonged survival times among all the treatment groups (mean survival time, 49.6 ± 11.5 days; Figure 4*B*).

Effect of Metronomic S-1 Chemotherapy Alone and in Combination with Vandetanib on Parameters of Tumor Angiogenesis

The results in Figure 5 show the MVD count in each treatment group. There was no significant difference in the MVD count between the control and the MTD S-1 group (control 41.1 ± 9.2, MTD S-1 35.8 ± 5.5; Figure 5*B*). However, tumor MVD was decreased in the metronomic S-1 group (17.2 ± 4.1) compared with the control group (P < .001) and the MTD S-1 group (P < .001; Figure 5*B*). Tumor MVD in mice treated with vandetanib was 13.7 ± 5.1. In the MTD S-1 plus vandetanib group, the MVD count was 18.8 ± 7.4. Metronomic S-1 plus vandetanib group showed the greatest reduction of tumor MVD (P < .01 compared with MTD S-1 plus vandetanib group, 8.2 ± 1.6; Figure 5*B*).

Detection of Proliferation and Apoptotic Cells in Tumor Tissues

To further investigate the mechanism of the observed antitumor effect, we examined the effect of metronomic S-1 and in combination with vandetanib on tumor cell proliferation and apoptosis (Figure 5). With respect to tumor cell proliferation, there were no differences between the control and all treated groups. The mean

number of apoptotic tumor cells (apoptotic index) measured in the control group was 6.2 ± 2.6. The MTD S-1 group did not show any significant difference (6.1 ± 4.9). However, the metronomic S-1 and vandetanib groups showed a significant increase in the apoptosis index (26.0 ± 5.4 and 18.4 ± 8.8, respectively, $P < .0001$). A significant increase in the tumor cell apoptosis index was also observed in the metronomic S-1 plus vandetanib group with 42 ± 3.5 ($P < .0001$).

Expression of VEGF and TSP-1 in Tumor Tissues

The results in Figure 6 show the expression of TSP-1 and VEGF in treated tumor tissues. The expression level of TSP-1 was significantly upregulated by approximately two- to three-fold in both the metronomic S-1 and the metronomic S-1 plus vandetanib treatment groups ($P < .05$ compared with the control group; Figure 6, *A* and *B*). With respect to expression levels of VEGF, there were no differences between the control and the MTD S-1 and metronomic S-1 groups (Figure 6, *C* and *D*). In contrast, the vandetanib and the metronomic S-1 plus vandetanib groups showed significantly upregulated the VEGF expression compared with the control group ($P < .05$; Figure 6, *C* and *D*). There was a significant difference between the vandetanib monotherapy group and the metronomic S-1 plus vandetanib treatment group ($P = .045$).

Discussion

Our results add to an expanding body of literature reporting the therapeutic benefit of metronomic chemotherapy, especially when it is combined concurrently with a targeted antiangiogenic drug [5,12,13]. Moreover, to our knowledge, this is the first preclinical report of using S-1 in a metronomic dosing and administration schedule for HCC preclinical model. Also noteworthy is that we undertook a comparative

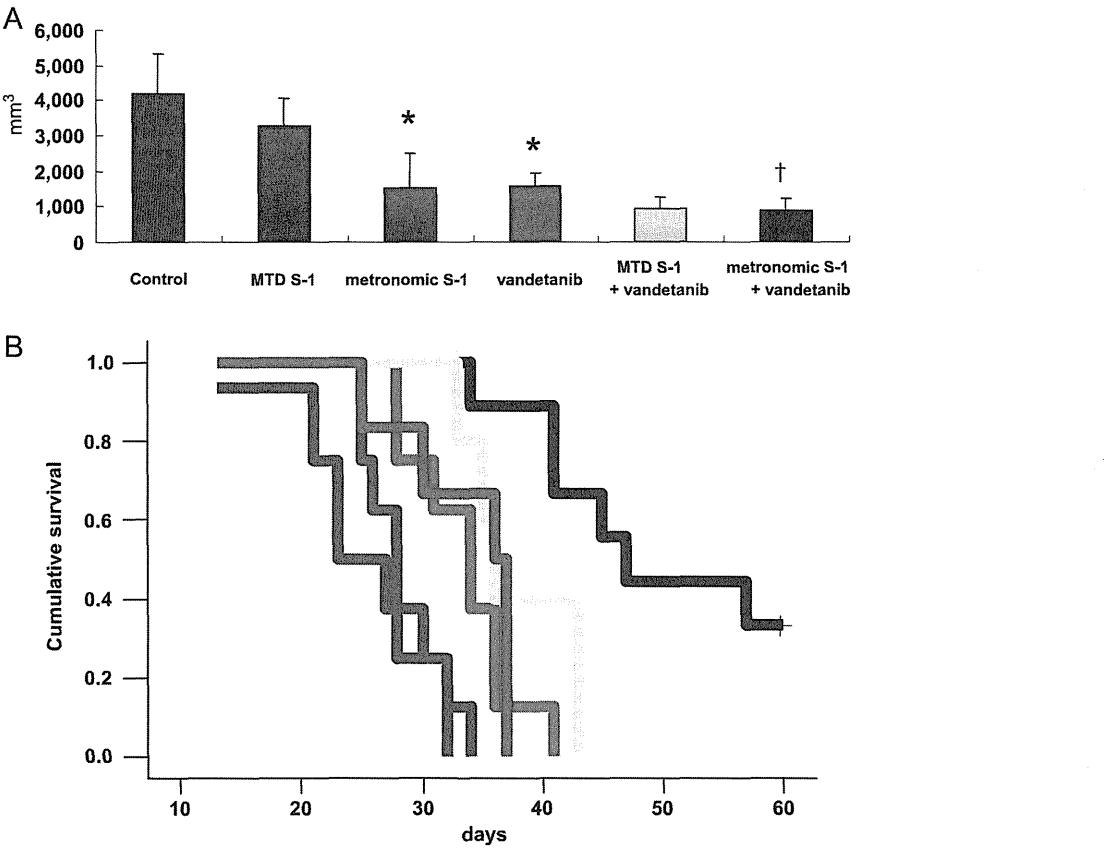

Figure 4. Assessment of therapeutic effects in KYN-2 liver transplant model. Tumor-bearing nude mice were treated in the following six groups: 1) HPMC as the control group (blue); 2) MTD S-1: 15 mg/kg per day for 1 week, followed by 1 week break period (purple); 3) metronomic S-1: 5 mg/kg per day for 2 weeks without break period (green); 4) vandetanib 25 mg/kg per day for 2 weeks (red); 5) MTD S-1 with vandetanib (yellow); or 6) metronomic S-1 with vandetanib (black). (A) Inhibition of tumor growth for KYN-2 liver transplant model. All treatments were performed 4 weeks in total. There was no significant difference between the control and the MTD S-1 groups. The metronomic S-1 group contributed to obvious inhibitory effect of tumor growth (*$P < .05$ compared with the control and the MTD S-1 groups). The metronomic S-1 with vandetanib treatment group showed the greatest inhibitory effect of tumor growth among all the groups (†$P < .001$). (B) Survival of mice treated with MTD S-1 or metronomic S-1 and in combination with vandetanib ($n = 10$ per group). Treatment was continued until mice were moribund, and days of life were recorded. Survival data were compared for significance with the log-rank test. MTD S-1 did not prolong survival compared with the control group. In contrast, metronomic S-1 prolonged survival compared with the control and MTD S-1 groups. The metronomic S-1 with vandetanib group provided the most effective therapy with longest survival times among all the groups ($P < .001$).